ELECTRIC COMMUTER TRANSPORT CONCEPT ENABLED BY COMBUSTION ENGINE RANGE EXTENDER

Georgi Atanasov [(1)], Jasper van Wensveen [(2)], Fabian Peter [(3)], Thomas Zill [(4)]

(1) German Aerospace Center (DLR), Institute for system architectures in aeronautics, Hein-Saß-Weg 22, 21129 Hamburg, Germany, georgi.atanasov@dlr.de, https://orcid.org/0000-0002-3235-1265

(2) Bauhaus Luftfahrt e.V., Willy-Messerschmitt-Straße 1, 82024 Taufkirchen, Germany Jasper.vanWensveen@bauhaus-luftfahrt.net, https://orcid.org/0000-0002-4644-0461

(3) Bauhaus Luftfahrt e.V., Willy-Messerschmitt-Straße 1, 82024 Taufkirchen, Germany, Fabian.Peter@bauhaus-luftfahrt.net

(4) German Aerospace Center (DLR), Institute for system architectures in aeronautics Hein-Saß-Weg 22, 21129 Hamburg, Germany, thomas.zill@dlr.de

Abstract

The low energy density of electric storage devices is currently the greatest hurdle for all-electric transportation by air. The main consequence of this low energy density is limited flight range. Whereas Lithium-Ion batteries have already reached sufficient energy density levels to be of practical use for automotive applications, the range limitation remains unpractical for air transport. A significant portion of the commercial commuter aircraft flights are operated on distances that could potentially be covered by all-electric aircraft. However, safety regulations prescribe diversion and holding requirements which push battery usage outside the feasible design space. Additionally, the design range of the commuter aircraft is usually much higher than the average range flown, as the range-flexibility allows for more efficient fleet operation and maintenance network setups. Adding a range extender to an aircraft that is capable of all-electric flight could potentially alleviate these issues. The range extender could be used for both providing Instrument Flight Rules (IFR) reserves capability and increased operational range, whilst enabling emission-free flight on shorter routes. This paper evaluates such a concept, named E19, through a conceptual aircraft design study based on state-of-the-art technology. The aircraft has a fully electric range of 190km with kerosene and the range extender providing the required IFR reserves and extra range when required. The fully electric range is able to serve roughly 50% of the commuter flights flown in 2018, whereas a stop-over with battery swapping strategy also enables full electric flight over longer distances.

Keywords: electric flight, local emission free flight, commuter aircraft, range extender, emission reduction

DECLARATIONS

Funding: N/A

Conflict of interest/Competing interests: N/A

Availability of data and material: N/A

Code availability: N/A

Authors' contributions: N/A

1. INTRODUCTION

The aviation industry faces severe challenges regarding its constantly growing environmental impact [1, 2]. Air vehicles have become significantly more efficient over the course of the last 50 years, resulting in a large CO_2 emissions reduction per revenue passenger kilometer [3]. However, the prospected growth of air traffic in the next decades [4, 5] will cause the global CO_2 emissions caused by aviation to rise significantly [2]. Hence, abandoning the combustion of fossil fuels during flight seems to be a feasible path to mitigate this rising impact. The introduction of electrical energy to substitute fossil fuels offers the potential to reduce emissions, at least on a local level. Unfortunately, battery powered hybrid and full-electric aircraft are still limited in their transport capability due to the low energy and power densities of batteries used for energy storage [6, 7, 8]. Even with moderate to optimistic projections of future battery performance, fully electric flight with batteries as the sole power source can realistically only be achieved over reduced, though still meaningful, flight ranges [9, 10, 11].

In 2018 the German Aerospace Center (DLR) and Bauhaus Luftfahrt teamed up in the Cooperation for Commuter Research (CoCoRe) project, to examine the possibilities and potential for hybrid-electric 19-seater aircraft. In particular

doi: 10.25967/490245

an answer was sought to the question whether it is possible to save travel time using commuter aircraft as a part of the transportation infrastructure and whether emissions can be reduced using a short-term hybrid-electric solution for this aircraft class. To answer these questions, the CoCoRe project was subdivided in two parts working closely: 1) a market and technological potential analysis, and 2) the conceptual aircraft design. The outcomes of the market analysis and technological potential have been presented in previous publications [12, 13]. An aircraft concept named E19 was the result of the second part of the project. A visualisation of the concept can be seen in Figure 1. The purpose of this paper is to present the conceptual aircraft design part, i.e. the conceptual design methodology used, as well as the final outcome of the aircraft design process.

Figure 1: Visualisation of the E19.

Commuter aircraft designed for 19 passengers typically operate at remarkably short flight distances [12]. Figure 2 shows that more than half of the operations in 2018 were flown on distances shorter than 200km. When purely considering these ranges, the majority of the flights could potentially be flown fully electric using state-of-the-art batteries. Nonetheless,

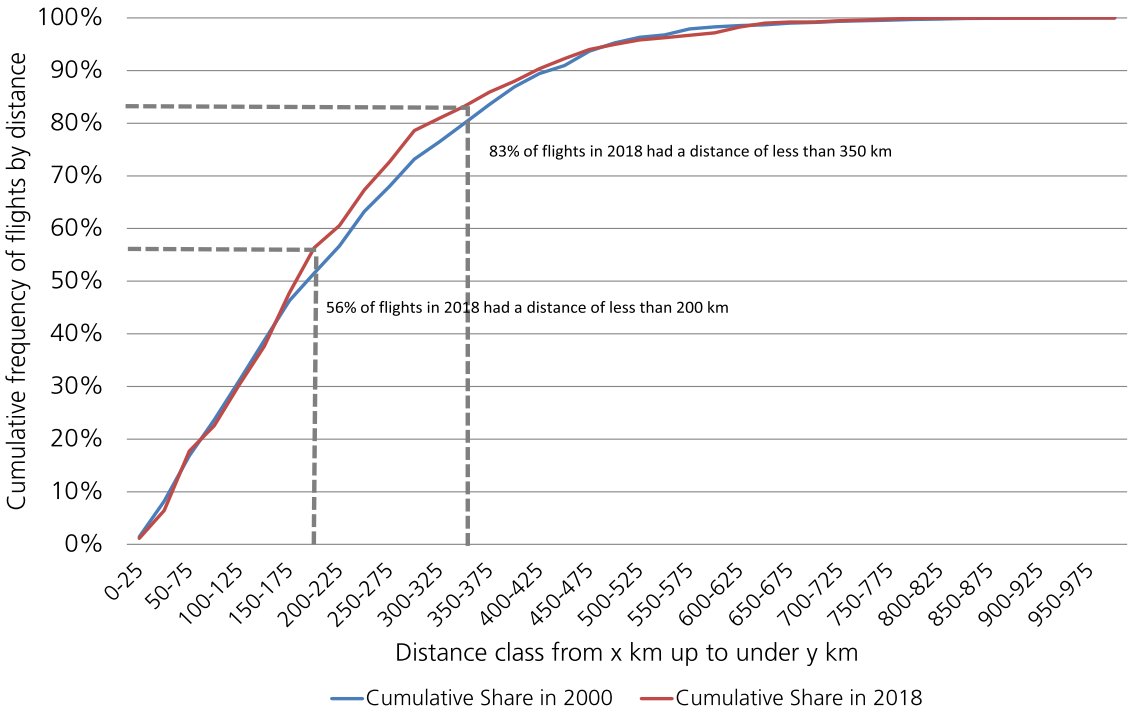

Figure 2: Cumulative share of scheduled passenger flights with 19-seater aircraft by distance in 2000 and 2018 [12].

safety regulations present a difficult obstacle, even for operation on such short flights. All IFR flights must be capable of a diversion mission and have an additional reserve for 45 minutes of flight time. This sets the bar too high for state-of-the-art battery technology and therefore requires some form of a hybrid solution.

Hybrid-electric propulsion has been researched extensively in the past. An elaborate literature survey on hybrid- and full-electric aircraft design approaches, models and concept has been published by Brelje and Martins [14]. Narrowing down the scope to full electric and hybrid-electric commuter aircraft, also here various design studies have been performed. The early NASA publications around full-electric and distributed electric propulsion and the importance of their integrated benefits, which would result in the X-57 demonstrator aircraft, already mentioned commuter aircraft as an application case; see for example [9]. In 2016 Fefermann et al. published a study that surveyed the potential of, and required technology targets for, a 19-seater aircraft while considering different propeller configurations [15]. In 2017 Juretzko et al. investigated the retro-fit of a RUAG Do228NG with a more conventional 2-propeller based hybrid-electric propulsion system and used a battery specific energy of 150Wh/kg while considering different mission hybridization strategies [16]. Tay et al. developed a software tool for flight performance and mission analysis of hybrid-electric aircraft and used it to analyse a hybrid-electric Do228 as well [17]. Kreimeier and Stumpf compared the variable operating costs of full electric, various hybrid-electric propulsion concepts, as well as conventional piston engine aircraft for on-demand air mobility applications [18]. Kruger et al. investigated the energy savings of a full electric and a hybrid-electric 20-seater aircraft compared to their conventional counterparts considering the cruise segment [19]. Finger et al. compared the conceptual hybrid-electric aircraft design approach used by FH Aachen University of Applied Sciences to the approach used by Delft University of Technology [20]. Subsequently both methods were used to design a hybrid-electric Do228, and the payload-range energy efficiency results showed a difference of only 5%. Narrowing down the scope to battery-based commuter aircraft capable of full-electric flight, whilst being fitted with a combustion-based range extender, some studies have been published in the past as well. In 2016 Jansen et al. presented a simple sizing study of a 9-seater commuter aircraft hybrid-electric powertrain with a 225kW range extender [21], using fixed efficiency and specific power figures. Their configuration utilises distributed electric propulsion in the form of wingtip propulsors and high-lift propellers. A sensitivity study shows a total propulsion system mass ranging between 1700 to 3300kg, depending on the technology performance assumptions. Stoll et al. published a conceptual aircraft design study on an 11-seat electric commuter aircraft with a range extender in the form of a diesel engine and advanced recuperative engine [8]. Two different configurations were analysed; both contained wingtip propellers, while one has an additional vertical tail plane mounted propeller, and the other high-lift propellers. They assumed a battery specific energy of 400Wh/kg on pack level. More recently, Orefice et al. performed the conceptual design of a 19-passenger hybrid-electric utilising distributed electric propulsion, similar to Stoll et al., to identify the optimum design range under multiple technological and certification aspects [22]. The RUAG Do228 was used as reference aircraft together with a battery specific energy of 500Wh/kg, presumably on pack level.

The E19 features an all-electric flight capability through Lithium-Ion batteries powered electric powertrain, for which the powertrain is sized using state-of-the-art technology assumptions. Gas turbines are integrated and sized to serve as range-extenders, giving the aircraft an increased range capability for improved operational flexibility. The mission reserves are also stored in the form of kerosene and used by the range extenders in case diversion is required. This approach allows the available battery capacity to be fully used during the main mission. The work presented here differentiates itself from the aforementioned hybrid-electric commuter studies in 3 ways to allow full electric flight and a fast entry-into-service:

1. A 19-passenger conventional twin-engine aircraft configuration integrating the battery and the gas turbines in nacelles located at the wing.
2. A fully electric mission capability with range-extenders for the mission reserves as well as longer mission ranges.
3. State-of-the-art technology assumptions.

The remainder of this paper is structured as follows: in Section 2 the reference aircraft and the Top-Level Aircraft Requirements (TLARs) for the E19 will be presented. The E19 configurational aspects and the reasoning behind them will be discussed in Section 3. The aircraft design methods, their applicability and validation, the general E19 design approach, as well as the mission calculation approach are presented in Section 4. Section 5 will present the E19 in terms of the design results, operational aspects, and the emission reduction potential. Conclusions and final remarks are given in Section 6.

2. REFERENCE AIRCRAFT AND E19 TLARS

In order to provide comparison data and a starting point for the aircraft design, three reference aircraft were chosen based on the results of the market analysis study (presented in [12, 13]), their technical specifications and mission capabilities. Commuter aircraft can be distinguished by a major design variation: a pressurized or unpressurized fuselage. This feature forms a trade-off between system mass and complexity, and the maximum possible cruise altitude of the aircraft. A higher cruise altitude in turn allows a higher cruise speed. The selection of reference aircraft for the study presented in this paper reflects this major distinction. The RUAG Do228 is a high wing aircraft propelled by two turboprop engines. Its first

flight was in 1981 and 270 units were produced [23]. Its distinctive rectangular fuselage cross section prominently displays its application on lower cruise altitudes in the form of a Short Take-off and Landing (STOL) utility purpose. This does not require a pressurized fuselage and hence, this aircraft represents the respective 19-seater aircraft class in this study. The Beechcraft 1900D is a low wing aircraft and driven by two turboprop engines. Its first flight was in 1982 and it features a pressurized fuselage, enabling cruise altitudes up to 7620m. With a unit count of 695 [24] it is one of the most produced type of this class, which is why it was chosen as the second representative reference aircraft. In addition to the B1900D an additional reference aircraft was chosen for the high speed/high altitude class. The British Aerospace Jetstream 31 shares most of the Beechcraft's characteristics. The main differences are that it features a three-abreast cabin layout and a cruciform-tail instead of a T-tail. An overview of the main design characteristics for each of the reference aircraft is provided in Table 1. The Jetstream aircraft is the smallest in terms of dimensions, whereas the Beechcraft is the heaviest. As can be seen, the pressurized aircraft also require higher engine power and usually feature a smaller wing optimized for high-speed cruise. The latter, however, increases the Take-Off Field Length (TOFL) and therefore imposes higher operational constraints on the aircraft. A full overview of active aircraft and use cases in this particular market segment can be found in the market analysis publication [12].

Table 1: Characteristics of the reference aircraft.

Characteristics	**Units**	**RUAGDo228NG** [25, 26, 27]	**Bae JS 31** [28, 29]	**Beechcraft 1900D** [30, 31, 32]
Wing span	m	16.97	15.85	17.64
Wing area	m^2	32.00	25.08	29.08
Total length	m	16.56	14.36	17.62
Propeller diameter	m	2.69	2.69	2.79
Engine type (2x)		TPE331-10GT/P	TPE331-10UF/G	PT6A-67D
OEM	kg	***3900	3450	4894
MTOM	kg	6400	6950	7766
MLM	kg	6100	6600	7605
Max. zero-fuel mass	kg	5940	6000	6879
Max. cruising speed	KIAS	223	263	277
Max. operating altitude	m	4572	7620	7620
Range with max. payload	km	396	-	585
Ferry range	km	2430	-	2306
Stall speed (full flaps & MTOM)	KIAS	66	86	84
$C_{Lmax,\ landing}$	-	2.55	2.26	2.29
$C_{Lmax,\ takeoff}$		1.95	1.8**	-
P_{max}	kW	1158	1402	1730
Wing loading	kg/m^2	200	276	270
P_{max} / MTOM	W/kg	181	202	223
TOFL	m	800	1440	1139

*With full flaps & MTOM **Difference between take-off and landing calculated from Reference [33] ***Incl. 2 pilots

The TLARs for the E19 are based on various considerations. The MTOM limit is set at the CS-23 certification limit of 8186kg to allow maximum battery mass, and therefore maximum fully electric range. Also, the number of passengers is fixed to the CS-23 limit of 19, resulting in a payload mass of 1805kg. In regard to the field lengths a longer TOFL and higher approach speed tend to relax the constraints on the wing and the engine sizing. This reduces the mass of these components, which in turn reduces the aircraft mass without fuel and battery. The latter can also be called the Maximum Zero Energy Mass (MZEM). Since for fully electric missions the fuel mass is determined only by the IFR reserves, a reduction in MZEM allows an increase in battery mass. For this reason, the more relaxed low-speed performance of the Jetstream 31 (see Table 1) has been chosen for the fully electric mission. It should also be kept in mind, that the E19 can potentially use the range extenders for take-off performance boost. However, the operational performance with regard to airport infrastructure was not studied in detail at this stage of the project. For this reason, the low-speed performance related aspects of the design were kept simple.

The TLARs of the E19 are summarized in Table 2.

Table 2: E19 Top-Level Aircraft Requirements (TLARs).

TLAR	Value	Unit	Remark
MTOM	8618	kg	CS-23 Limit
Max. payload	1805	kg	Equals BAe Jetstream 31
Min. cruise altitude	3048	m	Standard CS-23 operating altitude
Ceiling altitude	7620	m	limit for pressurized cabins
Diversion mission	185	km	IFR safety regulations
Approach speed	56	m/s	Equals BAe Jetstream 31
TOFL	1440	m	Equals BAe Jetstream 31

3. E19 CONFIGURATIONAL ASPECTS

This section will describe the reasoning behind the overall aircraft configuration chosen for the E19, of which a visualisation can be seen in Figure 1. The low-wing configuration allows integration of the batteries inside the nacelle and on top of the wing with the landing gear located directly underneath. Through this setup, the battery mass, which constitutes a significant portion of the total aircraft mass, is directly supported by the undercarriage minimizing the loads on the wing structure during hard landing. The battery location also significantly reduces the wing root bending moment during flight. Furthermore, it is located near the Centre of Gravity (CoG) of the empty aircraft, which is favourable in terms of reduced CoG travel between different payload configurations. The electric motors and the range extenders are also integrated in the nacelles between the propeller and the wing leading edge. To avoid space allocation conflicts with the propulsion chain, the landing gear retracts towards the fuselage, similarly to the Jetstream 31. The E19 features a pressurized cabin for high-altitude flight. Electric aircraft have inherently high service ceiling capabilities due to the absence of power lapse with altitude of the electric propulsion components. As such, top of climb is generally no longer the sizing condition for the installed power of the propulsion chain. This allows a higher design cruise altitude without the usual trade-off with engine size. The basic fuselage geometry is assumed to be the same as the Jetstream 31 with a slight modification to the nose shape to house the new landing gear with updated dimensions. The landing gear sizing considers the propeller ground clearance of the Jetstream 31 as minimum, and at least a 12° take-off rotation angle. A conventional empennage arrangement tends to be the lightest solution and one with good aerodynamic properties. The main drawback of this arrangement is that the horizontal tail is located directly in the propeller wake. This can have a negative effect on structural fatigue, which can be an acceptable trade-off for the improved performance, as indicated by the Do228 design. Ultimately, the E19 configuration is very similar to that of the Jetstream 31, which was also one of the main reasons for it to be included as a reference aircraft.

4. DESIGN METHODOLOGY

The overall aircraft design methodology used for this study is on a conceptual aircraft design level. The aircraft design framework openAD [34] is used as a backbone for the modelling of the E19. It has been developed by the DLR and is based on well-understood and mostly publicly available handbook methods. Furthermore, it has enhanced capabilities on the design and thermodynamic cycle calculation of turbofan and turboprop engines. OpenAD can be used for overall aircraft calculations and sizing, design space explorations and parameter optimizations. It is composed by a broad parameter set describing the entire aircraft design without a predefined input to output schema, i.e. the input parameter set is not fixed. This allows feeding results from higher-fidelity tools, or simply from supplemental tools, back into the overall aircraft sizing process. Thus, it can be used as an overall aircraft design synthesizer within a broader multifidelity design environment for evaluation and assessment various concepts and technologies.

For the E19 study, openAD is used to calculate the aircraft mass breakdown and the aerodynamic properties of the aircraft, as well as for the range-extender sizing and the reserve mission fuel calculation. Since openAD does not feature a capability for modelling a hybrid-electric propulsion system, the latter is sized in a separate script outside openAD. The results are fed back into openAD for the next calculation loop and the process is repeated until convergence.

The openAD model used for the E19 as well as its validation are described in Section 4.1, followed by model constraints in Section 4.2. The electric propulsion technology assumptions are given in Section 4.3. The overall sizing loop for the E19 is described in Section 4.4.

4.1. Set-up and validation of the E19 openAD model.

An openAD model of the Do228, refined throughout previous DLR internal projects, was available for the CoCoRe project. This model featured a thorough calibration of the parameterized calculation of the component masses, aerodynamic properties and engine performance, based on the internal data of the Do228. This calibrated model was used for sizing the E19 with only minor modifications required in the component mass calculation due to the configurative

differences between the two aircraft. The overall E19 model was validated by calculating the overall characteristics of the Jetstream 31 and the B1900D, as both aircraft feature a configuration similar to the E19. As a first step, the overall geometry and TLARs of each the two aircraft were set using the data available in the references on the JS31 [28, 29] and the B1900D [30, 31, 32]. The calculation of the mass breakdown and the high-speed performance as well as the validation of the results are described in detail in the following subsections.

4.1.1. Mass breakdown

OpenAD uses handbook methods from [35, 36, 37] to estimate the mass of each major aircraft component. Some components utilize different mass functions depending on the aircraft type or class. For the current study, a set of component mass functions is selected according to the specifics of the 19-passenger commuter turboprop class. The tailored openAD mass model was calibrated on the Do228 aircraft component mass breakdown data from an internal project. The parametric mass functions used for the major components include dependencies for the main configurational differences between the Do228 and the E19. Most noteworthy is a wing mass function from the LTH [38]. Beside the main dependencies on top-level geometrical parameters, (e.g. wing area, aspect ratio, average wing sweep angle, airfoil thickness, aircraft mass and dive speed), the function differentiates between landing gear and engine installation on the wing or fuselage. It also includes a dependency for additional masses installed on the wing, which allows for a first estimation of the effect of battery integration within the nacelles. The LTH method itself has been validated on approximately 60 aircraft ranging from 6-seater propeller aircraft to large transonic airliners with four engines like the A340 and Boeing 747, and has a standard deviation of 14% [38]. During the design process limits were imposed on the aircraft design parameters of E19 (e.g. an aspect ratio limit of 12) to ensure that the wing mass calculation remains within the value ranges of the datapoints considered for the parametric function. Similar to the wing function, the mass function for the fuselage includes configurational aspects like the wing and landing gear location, and also takes into account cabin pressurization.

The landing gear mass function depends on the Maximum Landing Mass (MLM) and the length of the landing gear strut [39]. This function is considered suitable for the E19 as it will account for the higher MLM of electric aircraft due to the battery mass remaining constant. This is also the only function that did not originally include a dependency on the configurational change between the Do228 and the E19, since it does not differentiate between fuselage-installed and wing-installed landing gear. To avoid underestimating the landing gear mass of the E19, the original calibration was corrected by a factor of 1.08, based on Torenbeek [35], to account for the installation at the wing.

The empennage mass function used in this study is not dependent on the empennage type. The Jetstream 31 features an cruciform tail, whereas the B1900D features a T-Tail. The Vertical TailPlane (VTP) structure requires reinforcement for carrying the Horizontal TailPlane (HTP) loads in both cases. This means that the mass function, calibrated on the conventional empennage of the Do228, is likely to be considerably underestimating the mass of the VTP for both these aircraft. However, this is not critical for the E19 modelling, as the aircraft configuration assumes a conventional empennage type, similar to the Do228.

All the aircraft system masses, apart from that of the Environmental Control System (ECS), were set identical to that of the Do228. The mass of the ECS was increased with 50% to account for the pressurized cabin. Furthermore, the sum of the furnishings and operator items was also assumed identical to the Do 228 model. In order to avoid disclosing confidential data, the total split between the system masses, furnishings, and operator items was slightly modified. Since these masses are assumed constant for the study, the modification in the split for the mass breakdown did not affect the results.

For the component mass breakdown validation, the fuel mass was set fixed to the difference between the MTOM and the Zero Fuel Mass (ZFM, which is the sum of OEM and the payload mass) of the design mission in order to decouple the performance effects on the overall mass. The result of the mass model validation is shown in Table 3. The validation shows an agreement with the top-level aircraft data of the reference aircraft, with OEM being under predicted by only 1.1% for the Jetstream 31 and by roughly 2.7% for the B1900D. The slight under prediction tendency is likely due to the empennage mass function not being suitable for empennage configurations different from the Do228. This will, however, not be the case for the E19.

Table 3: Mass model validation results.

Component	Units	BAe JS31 [28, 29]	B1900D [30, 31, 32]
Wing	kg	794	882
Fuselage Structure	kg	772	897
HTP	kg	103	106
VTP	kg	69	64
Nacelle & Pylon	kg	213	222
Landing Gear (Main + Nose)	kg	302	275
Propulsion	kg	665	923
Gas Turbine	kg	*349*	*488*
Propeller	kg	*202*	*275*
Systems (Engine)	kg	*114*	*160*
Systems	kg	650	650
Furnishings	kg	270	270
Manufacturer's Empty Mass	**kg**	**3838**	**4288**
Operator's Items	kg	475	475
Operating Empty Mass (OEM) - model result	**kg**	**4313**	**4763**
OEM Target (reference data)	**kg**	**4360**	**4894**
Deviation from OEM Target		**-1.1%**	**-2.7%**
Max. Payload	kg	1805	1985
Max. Fuel	kg	1372	2022
Max. Takeoff Mass (MTOM) - model result	**kg**	**6903**	**7638**
MTOM Target (reference data)	**kg**	**6950**	**7766**
Deviation from MTOM Target		**-0.7%**	**-1.7%**

4.1.2. Turboprop engine performance model.

OpenAD is able to perform simplified engine cycle calculations, which calculates the overall fuel efficiency in cruise as well as the power and efficiency lapse for other operating points [34]. The engine performance of the Do228 and the Jetstream 31 are calculated with the identical model set-up, since they have a similar engine. The engine model was used for the B1900D calculation as well, despite the different engine types, as no other suitable model was available. The same parametric engine model is also used to size the range extenders of the E19.

4.1.3. Aerodynamics

The aerodynamic model implemented in openAD is based on the handbook methods provided in [35, 37, 40]. It has been used, refined, and validated through multiple DLR aircraft design projects depicting various aircraft types and classes [34], including the Do228. The calibrated Do228 aerodynamic calculation model is used for the E19 design. Figure 3 shows the reference aircraft aerodynamic calculation results in the form of L/D vs cL performance for the cruise conditions of each respective aircraft.

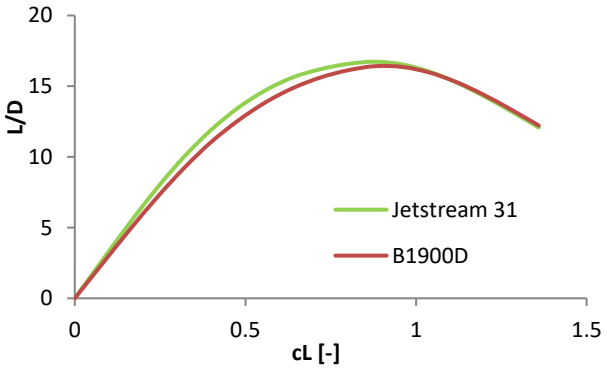

Figure 3: openAD calculated aerodynamic polars for the Jetstream 31 and the Beechcraft 1900D.

4.1.4. Payload-Range validation

The openAD sizing loop includes a mission performance calculation. As a validation of the overall high-speed performance calculation, which uses the engine model described in Section 4.1.2 and the aerodynamic model described in Section 4.1.3, the payload range diagrams for the Jetstream 31 and B1900D were calculated and compared to the

reference aircraft data. The comparison is shown in Figure 4. The Jetstream 31 model could replicate the single available data point from [41] for the aircraft without engine or aerodynamic model calibration with less than 1% deviation. The performance of the B1900D was calculated around 8% better compared to the available data points from [30]. However, there is a higher uncertainty in the calculation of this aircraft, as the engines of the Beechcraft 1900D are from a different manufacturer than those of the Do228, with which the model was calibrated

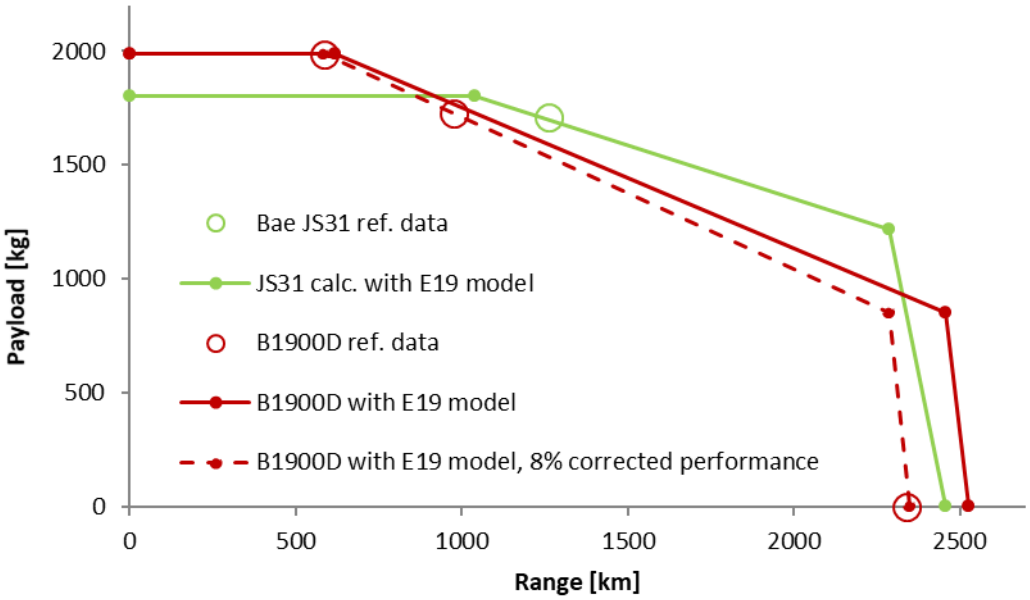

Figure 4: Payload-range diagram calibration of the Jetstream 31 and Beechcraft 1900D.

Additionally, the B1900D has various additional stabilizing surfaces (i.e. HTP attached vertical fins and fuselage attached horizontal fins) that are not present on the Do228 and Jetstream 31. These surfaces are not accounted for in the aerodynamic models, although they create additional drag. Hence, in order to meet the payload-range diagram data points, both the engine model and the aerodynamic model are evenly readjusted (each by approximately 4%). The resulting consistent match of the Beechcraft 1900D payload-range points by the calculation model shown in Figure 4 is an indicator of the reliable mission performance calculation of openAD.

4.2. E19 openAD model constraints

In contrast to the reference aircraft calculation, the geometry of the E19 is not fixed. It is an outcome of the overall sizing of the aircraft, which will be described in Section 4.4. The only exception is the fuselage of the E19, which is modelled after the geometry of the Jetstream 31 fuselage without parameterization.

An important boundary condition used for the modelling is that the MTOM is always set fixed to the CS23 certification limit of 8618kg. This design simplification ensures the maximization of the battery size that can be carried without exceeding the certification limit, thereby maximizing achievable electric range of the aircraft.

The wing modelling assumes a simple trapezoid with a fixed taper ratio of 0.4 and an unswept 50% chord line. The thickness and twist distribution were set fixed without optimization, since the lift-dependent drag was modelled to reproduce the behaviour of Do228 with only the aspect ratio as a free parameter. A minimum stability static margin of 0.1 was set for the wing positioning.

The wing reference area is used as an input parameter that is converged in the overall sizing loop, which will be described in detail in Section 4.4. The aspect ratio as well as the maximum lift coefficients for the take-off and the landing calculations are set as top-level inputs that could be used for design studies by the user.

The empennage surfaces also assume a simple trapezoid form, with the HTP resembling the Do228 HTP planform. The VTP planform was based on the Jetstream 31 VTP shape, mostly for consistency with the fuselage geometry and the structural attachment of the VTP. As the E19 features the same empennage type as the Do228, the HTP volume coefficient is set identical to the Do228 model. The VTP reference area was used as a free input, which is determined in the overall sizing loop as will be described in Section 4.4.

The propeller design and the take-off power to propeller disk area ratio are assumed to be identical to that of the Jetstream 31. This simplified approach was taken since the resulting E19 propeller shaft power level is similar to that of the Jetstream 31, as will be shown in the results later on. The landing gear length is sized to provide the same propeller ground distance as the Jetstream 31.

The sizing point for the range extenders is loiter-speed operation at 3048m. It is assumed that they are decoupled from the propeller shaft when the E19 operates at a fully electric mode and can be coupled to the propeller shaft to provide power in parallel to the electric motors when required. The specific mass and the thermodynamic efficiency inputs are equal to those used for the Do228 engines. A mass penalty of 10% is set in the gas turbine mass calculation to account for the shaft clutches. The mission reserves, which are assumed to be carried out by the range extenders, are also calculated within the openAD model.

All the propulsion components of the E19, including the battery, are located within the nacelles as shown in Figure 5. Therefore, the nacelle geometry is driven by the space allocation considerations of the propulsion system integration. Only the nacelle diameter is used as an input in the openAD model.

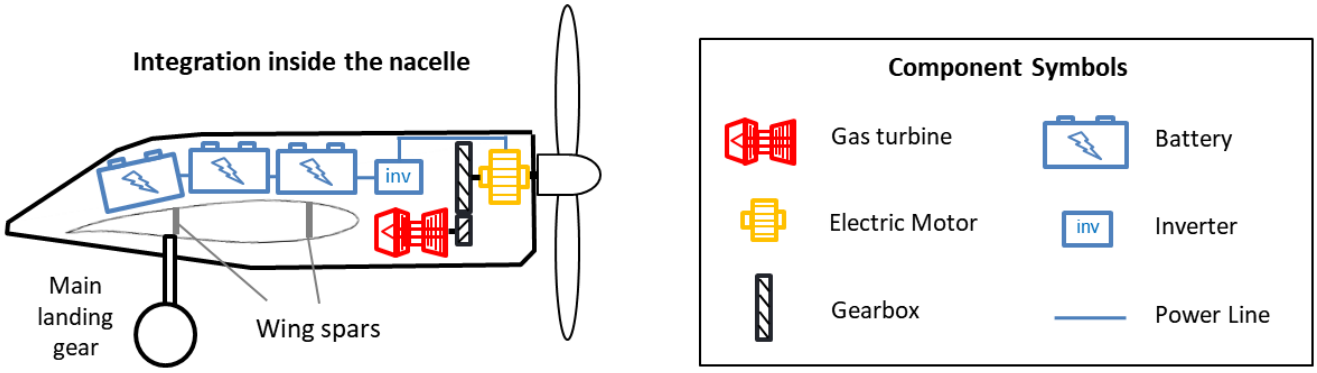

Figure 5: Propulsion system integration.

The mass budget for the hybrid-electric powertrain is calculated as the difference between the fixed MTOM of the aircraft and the sum of the other aircraft components, the maximum payload mass and the calculated kerosene mass required for the mission reserves. The powertrain is sized and the resulting battery mass calculated through a secondary script within the overall design loop as described in Section 4.4

4.3. Electric propulsion technology assumptions

State-of-the-art technology with technology readiness level 6+ (i.e. at or beyond technology demonstration) is used for the sizing of the electric propulsion system components. The electric motor specific power assumption is based on two motors from the Siemens products and prototypes portfolio [42]. The SP260D-A has the highest specific power of 5.9kW/kg achieved at 2500RPM, while the SP200D has a specific torque of 30.6Nm/kg at 1300RPM. The propellers of the E19 are set to operate at 1600RPM. In order to include the apparent compromise between specific torque and maximum RPM, the specific torque and power achievable by the motor is estimated through linear interpolation of the maximum rotational speed between the data points of the SP260D-A and the SP200D.

The battery assumptions are provided in Table 4. The model assumes a battery pack specific energy of 230Wh/kg, which is claimed in reference [43]. The French battery pack manufacturer TYVA claims a similar energy density for a battery pack to be used in an electric aircraft prototype [44, 45]. Usually, the specific energy of the battery is a trade-off with the achievable specific power, even for different discharge rates of the same battery. Modelling such characteristics behaviour was outside of the scope of this conceptual study, and as a simplification the specific energy was kept constant and no discharge rate effects were considered. The maximum C-rate of 3.0 means that the batteries can be fully discharged in 20 minutes (1/3h). The assumption of the specific energy being independent of the discharge rate then implies a specific power of the battery of around 690W/kg. The model takes into account battery operation between 90% State of Charge (SoC) at the start of a normal mission and a minimum of 20% SoC at the end of a normal mission. This reduces the useful specific energy to around 160Wh/kg. In the context of this paper a normal mission is defined as one without diversion or component failure. Additionally, 1000 operational cycles at the normal operating conditions are assumed, as well as 90% charge-discharge efficiency [46].

The power controller sizing considers a specific power of 115kW/kg based on the data from the Siemens products portfolio [42, 47]. The efficiency of the power controller is assumed to be 98% [48]. The power distribution system,

which includes the power cables, bus bars, and circuit breakers, is allocated 40kg at a powertrain output of 1MW. For the parameterized sizing, this mass is scaled linearly with the maximum required power output of the E19. A power cable efficiency of 99.7% is assumed. The thermal management system is sized using a specific power assumption of 2kW/kg, based on [49].

Table 4: Battery pack technology assumptions on system level.

Parameter	Value	Unit	Remarks
Specific energy	230	Wh/kg	Inc. casing and systems
Specific power	690*	W/kg	Based on [43]
Start state of charge	90	%	In normal operation
End state of charge	20	%	
Useful specific energy	161	Wh/kg	Available for the mission
End-of-Life cycles	1000	-	Assuming operation between 90% and 20% nominal SoC
Charge-Discharge Efficiency	90	%	Based on [46]

*3C capability for the 230Wh/kg battery pack was stated during the presentation of [43]

Since the nacelle size depends on the volume of the propulsion system components, a simplified modelling of the space allocation, dependent on the total volume of the components, was performed. The volume of the propulsion system components is determined by the volume-specific power and energy assumptions summarized in Table 5. The assumptions for the e-motor and inverter are taken from the Siemens products and prototypes data [42, 47, 50], whereas the battery pack volume is calculated by a volume-specific energy figure taken from a TYVA product catalogue [45]. The volume-specific power of the range extender is derived from the geometry of the Honeywell turboprop engine TPE-331-10U. Only the dimensions of the main gas turbine body were taken into account, with an approximate length and diameter of 90cm and 50cm respectively [51]. The engine is capable of delivering a shaft power of 660kW, which results in 3.7kW/l for a simplified cylinder form. The range extender diameter to length ratio is assumed identical. The gas turbine is located at the lower part of the nacelle to allow for the integration of an air inlet and exhaust below the electric components.

Table 5: Overview of the component volumetric assumptions

Component	Volume-Specific Power / Energy	Comment
E-Motor	6.3 kW/l	
Inverter	160 kW/l	
Battery Pack	360 Wh/l	Incl. systems
Gas Turbine	2.2 kW/l	Without systems
Gearbox & Clutch	3.1 kW/l	With the casing

4.4. E19 overall sizing loop

The openAD model described in the previous subsections is used in a convergence loop with a separate script, which uses the openAD model output to calculate the electric propulsion components characteristics. Despite the fixed MTOM input, the loop is still necessary in order to converge the design, as will be described in the following subsections. The wing aspect ratio as well as the take-off and landing maximum lift coefficients are used as fixed inputs for the entire convergence process.

4.4.1. Sizing of the electric propulsion system components.

All electric operation capability is a target for the E19 design. No hard constraints are set for the cruise or climb speed of the aircraft, therefore the sizing power for the electric propulsion system components comes from the take-off requirement from Table 2. Roskam provides an empirical method for estimating the TOFL performance of an aircraft, which can be summarized with the following dependency:

$$TOFL = f(TOP), where\ TOP = \frac{TOM^2}{S_{ref} \cdot P_{SH,tot} \cdot c_{L,maxTO}} \quad (1)$$

Where:

TOFL	Take-Off Field Length
TOP	Take-Off Performance parameter
$P_{SH,tot}$	Total shaft power of the aircraft
S_{ref}	Wing reference area
TOM	Take-Off Mass
$c_{Lmax,\ TO}$	Maximum takeoff lift coefficient

From Equation (1) follows that in order to achieve the same TOFL, TOP needs to remain constant. Since the TOFL TLAR is set identical to the Jetstream 31, its TOP, calculated with the data shown in Table 1, is used for the power requirement calculations.

The sizing of the electric propulsion components follows the following procedure:

- Step 1: As described in Section 4.2, the wing reference area is used as an input in the openAD model. Hence, after the openAD model is converged, the power requirement needed to meet the TOP constraint is calculated for this reference area.
- Step 2: The power requirement is used to calculate the mass and volume of the electric motors, inverters, power distribution and cooling system.
- Step 3: The total mass that is allocated for the electric propulsion system resulting from the openAD calculation is calculated as the difference between the fixed MTOM of the aircraft and the sum of all other aircraft components, the maximum payload mass and the calculated kerosene mass needed for the mission reserves (see Section 4.2). The battery mass is calculated by subtracting the mass calculated in step 2 from the total electric propulsion system mass.
- Step 4: The calculated battery mass is used to determine the maximum battery power output and its energy capacity using the assumptions from Table 4.

For the next convergence calculation loop, the openAD input is modified. The power calculated in step 1 is used to adjust the openAD input of the propeller diameter, whereas the nacelle diameter is adjusted with respect to the total calculated volume of the components. The VTP reference area is calculated to ensure the same one engine inoperative (OEI) using the Do228 data as a reference and correcting for sthe VTP lever arm, dynamic pressure during the second segment climb, the maximum thrust of the operating engine and the spanwise position of the engine. A yaw stability assessment was not performed for the study. The wing reference area input is also modified dependent on the power requirement calculated in step 1 and the power capability of the battery calculated in step 4. The wing reference area convergence will be explained more in detail in the following subchapter.

4.4.2. Converging the E19 design

The convergence of the E19 design depends on the optimization strategy chosen in the modelling, which is the optimization of the electric range of the concept. Since there is no hard requirement for the cruise speed of the aircraft and due to focus on the efficiency optimization, the cruise speed is rather only a result of the wing reference area and the cruise lift coefficient, which is chosen to be close to the best aerodynamic efficiency (see Section 4.5 for more details). Due to the fixed aspect ratio, a bigger wing tends to improve the aerodynamic efficiency in cruise, as the wing span increases (despite constant MTOM) and furthermore the total wetted area of the aircraft with respect to the wing reference area decreases. However, a bigger wing also increases the MZEM, which reduces the battery mass to not exceed the MTOM limit of 8618kg. As a result of these two opposing effects, the wing reference area has a relatively low impact on the overall energy efficiency of the aircraft, which is also shown in the sensitivity study results in Section 5.6. Nevertheless, a smaller wing has a positive overall impact on the results. Hence, the optimization strategy for the design convergence was reduced to choosing the minimum wing area that can meet the low-speed TLARs. For each loop of the design convergence, the wing size is adjusted such that the required and available power of the battery are matched. A hard constraint for the wing reference area is meeting the approach speed requirement. Since the wing size effect on the overall results of the study was estimated to be relatively low, the modelling effort on the low-speed performance was limited to the TOP parameter from Equation (1) and the approach speed constraint calculation.

4.5. E19 mission calculation

The mission calculation takes place is a separate script after the design is converged. The aircraft data from the openAD output, as well as the propulsion system sizing described in Subsection 4.4.1 are used as inputs for a simple iterative mission calculation model. The main goal of the model is to determine the achievable range for a given battery energy, fuel, and payload. The calculation assumptions for the main mission phases, namely climb, cruise, and descent, are as follows:

- During fully electric climb, the motors operate at maximum continuous power.
- The cruise speed is not a TLAR but an optimization parameter, which ensures a good aerodynamic performance in cruise regardless of the wing loading of the aircraft. Different cruise speed optimization strategies were applied for the all-electric and the hybrid missions, which will be discussed in the results (see Section 5.3).

- If kerosene is required for the normal mission, the range extenders are running at maximum rating during climb, whereas the battery supplements as much as needed to achieve the take-off shaft power on the propellers.
- During cruise the battery and the range extenders are running at a fixed power split, which is calculated such that both deplete the energy available for cruise simultaneously. A constraint is that the gas turbines cannot exceed their maximum cruise power.
- The aircraft climbs to the highest altitude possible at which the range extenders and the battery are still able to provide the required power for the cruise phase at a lift coefficient optimized for the mission and with a power split as described in the previous point. This approach allows optimizing the trade-off between the achievable range and the mission time as described in Subsection 5.3.2.
- During descent the aircraft glides at a designated lift coefficient, which results in a constant calibrated air speed descent. A drag penalty is assumed for the feathered propellers, which is calculated according to Roskam [52]. For the E19 this results in approximately 20 drag counts, or roughly a 5% drag penalty in descent.
- Off-takes equivalent to 20kW propeller shaft power are assumed for the missions in which the aircraft climbs higher than 3048m.
- It is assumed that taxi, take-off, approach and landing are performed fully electrical. The assigned allowances are summarized in Table 6. Furthermore, a contingency of 5% for each energy storage type that is used for the mission is added.

Table 6: E19 design mission allowances.

Segment	Time [min]	Energy [kWh]
Taxi out	3.0	0.8
Take-off	1.1	24.7
Approach & Landing	2.0	6.1
Taxi in	3.0	0.8
Total	**9.1**	**32.4**

5. RESULTS AND DISCUSSION

This section provides an overview of the overall aircraft design result of the E19. The design optimization process is discussed in Section 5.1. Section 5.2 provides the main aircraft characteristics, including a 3-view, mass breakdown, the space allocation within the nacelle and cruise aerodynamic performance. The mission analysis results are discussed in Section 5.3. A discussion on the operational aspects of the aircraft is provided in Section 5.4, which is followed by an assessment of the capabilities of E19 with regard to the global 19-passenger aircraft utilization perspective in Section 5.5. Finally, a results sensitivity discussion is presented in Section 5.6.

5.1. Design optimization

The main design focus of the study is the maximization of the electric range of the aircraft for the assumed state-of-the-art electric propulsion technology. The aspect ratio of the wing is an important design parameter in this regard. Since there is no hard constraint on the wing span, a preliminary design study was performed, which showed that an optimization would result in an unusually high aspect ratio. However, as described in Section 4.1.1, a limit for the aspect ratio of the wing of 12 was set in order to reduce the uncertainties in the wing mass estimation.

Setting a fixed aspect ratio of 12 only leaves the reference area to be optimized. The optimization of the wing reference area and the high-lift system is a complex trade-off between a good aerodynamic efficiency for a cruise speed requirement optimized for operating costs, low speed performance requirements that offer sufficient operational flexibility and the minimization of the propulsion system mass (i.e. cost). However, a cost optimization is outside of the scope of the current study. Furthermore, as will be shown in Section 5.6, the wing reference area does not significantly affect the overall study results, which focus on outlining the efficiency potential of an electrically driven aircraft for the commuter aircraft fleet. Hence, the overall effort on the low-speed performance optimization was kept low. However, assuming the same maximum lift coefficient to the Jetstream 31, resulted in a design with a relatively big wing with a reference area of over 40m^2, which also resulted in a poor performance in terms of cruise speed compared to the reference aircraft. When it comes to electric aircraft design, there are a number of design measures that can be used to improve the take-off performance:

- The electric components of the propulsion chain can be overpowered for a short time, especially for the duration of the take-off run, which is around 30 seconds and the components temperature is still low before the start (cold start).

- The relatively low take-off power of the E19 design is due to the limited power capability of the high-energy battery. However, a battery design with a booster high-power battery, which could be used to improve the overall take-off performance is possible.
- Distributed propulsion architecture could be used for reducing the OEI requirements of the aircraft.

The modelling of any of these options would unnecessarily increase the complexity of the study, given the mentioned low overall impact on the results. A lower-effort optimization was done with regard to the maximum take-off lift coefficient. The design was calculated for higher take-off lift coefficients with a post-convergence check of the OEI performance, using simplified handbook methods of Roskam [52] for the calculations. As a simplification, a complete engine loss, including the battery of one nacelle was assumed for the calculations. The calculations were performed for ISA conditions with an assumed power oversizing of 20% in order to allow for take-off at higher altitudes, which would ensure some operational flexibility. It was estimated that these constraints could be fulfilled for maximum take-off lift coefficients up to 2.35. Hence, in order to minimize the wing size, a maximum take-off lift coefficient of 2.35 was set for the final design.

The value is unusually high when compared to the conventional turboprop values shown in Table 1. However, it must be kept in mind that the take-off maximum lift coefficient is an optimization variable, which strongly depends on the design constraints of the aircraft.

The same maximum landing lift coefficient as for the Do228 of 2.55 is assumed (see Table 1). It is shown in Figure 6, that even with the high take-off lift coefficient assumption, the approach speed constraint is still not critical for the design.

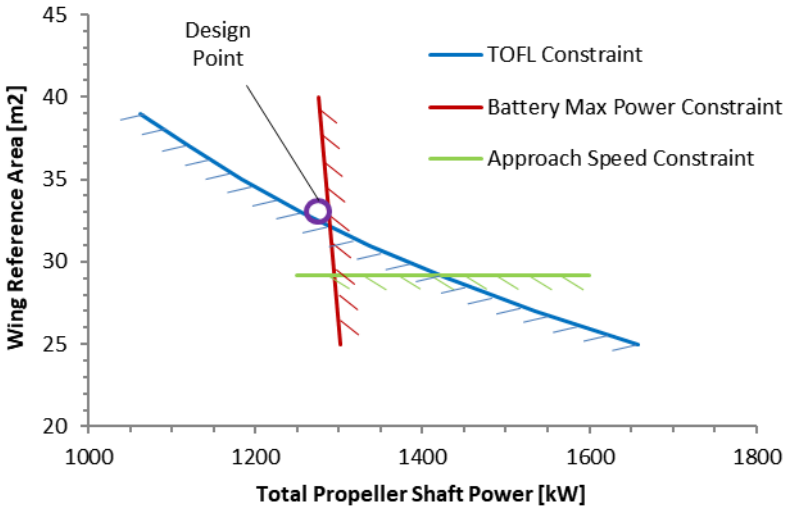

Figure 6: E19 wing reference area sizing constraints.

5.2. E19 aircraft characteristics

The overall dimensions of the E19, which result from the models and assumptions described in Sections 3 and 4, are provided in Figure 7. The main wing has a span of 20m, an area of 33.2m^2 and an aspect ratio of 12. With a total length of 15.19m, the aircraft is slightly longer than the Jetstream 31. The mass breakdown of the E19 is given in Table 8, whereas Table 7 provides an overall summary of the basic characteristics of the hybrid propulsion chain components.

Table 7: E19 hybrid-electric powertrain component properties summary.

Component	Total mass [kg]	Total power [kW]	Efficiency [%]	Remarks
E-Motors	253	1251	95.0	4.94kW/kg @1680RPM
Controllers	12	1321	98.0	-
Cooling	44	89	-	For e-motor & controller.
Power Distribution	66	1321	99.7	Including thermal management
Battery	2018	1352	85.0	Charge-discharge cycle efficiency
Range Extenders (incl. gearbox & systems)	260	600*	22.0**	

*ISA sea level condition **Incl. gearbox & clutches

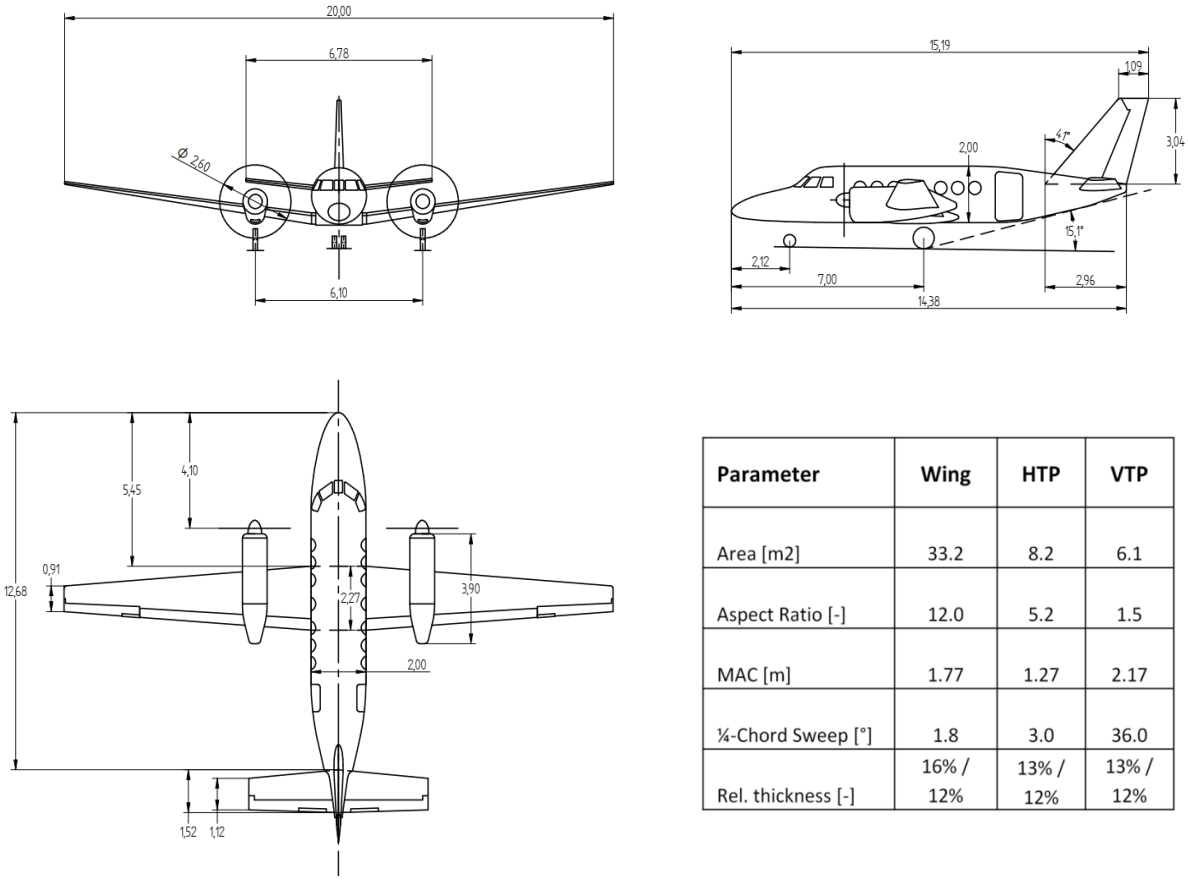

Parameter	Wing	HTP	VTP
Area [m2]	33.2	8.2	6.1
Aspect Ratio [-]	12.0	5.2	1.5
MAC [m]	1.77	1.27	2.17
¼-Chord Sweep [°]	1.8	3.0	36.0
Rel. thickness [-]	16% / 12%	13% / 12%	13% / 12%

Figure 7: Three-view of the E19.

Table 8: E19 mass breakdown.

Component	Unit	Value
Wing	kg	984
Fuselage Structure	kg	703
HTP	kg	97
VTP	kg	49
Nacelle & Pylon	kg	249
Landing Gear	kg	364
Structure	**kg**	**2446**
Propeller	kg	138
E-Motor	kg	253
Power Controller	kg	12
Power Distribution	kg	66
Cooling	kg	44
Range Extenders (incl. clutches)	kg	150
Range extender subsystems	kg	100
Propulsion	**kg**	**763**
Battery	kg	2018
Aircraft subsystems	kg	650
Furnishings	kg	270
Manufacturer's Empty Mass	**kg**	**6146**
Operator's Items	kg	475
Operating Empty Mass (OEM)	**kg**	**6621**
Max. Payload	kg	1805
Max. Zero-Fuel Mass (MZFM)	kg	8426
Design Fuel (IFR reserves only)	kg	192
Max. Fuel	kg	1997
Max. Takeoff Mass (MTOM)	**kg**	**8618**
Max. Landing Mass (MLM)	**Kg**	**8618**

As mentioned in Section 3, the nacelle geometry is designed for accommodating the entire propulsion system. A geometrical analysis was performed at a basic level, and the space allocation is shown in Figure 8. To avoid underestimation of the nacelle size, considerable margins were used for the design. All components assume at least 5cm offset from the outer skin of the nacelle. An offset of 10cm was used for the gas turbine installation. With the volume-specific energy of the battery pack of 360Wh/l, the overall battery pack volume per nacelle would be around 0.7m^3. However, the nacelle sizing assumed a volume of 1m^3 as a compensation for any integration difficulties that could result from installation of non-specifically tailored battery shapes. Additionally, 0.25m^3 volume was allocated for the integration of power management and thermal management systems. Especially the later will play a crucial role, but has not been considered in detail during this study.

The payload range characteristics of the aircraft are shown in Figure 9. With full payload and IFR kerosene reserves, no kerosene can be allocated for the main mission, as the aircraft reaches its MTOM limitation. Under these conditions, the

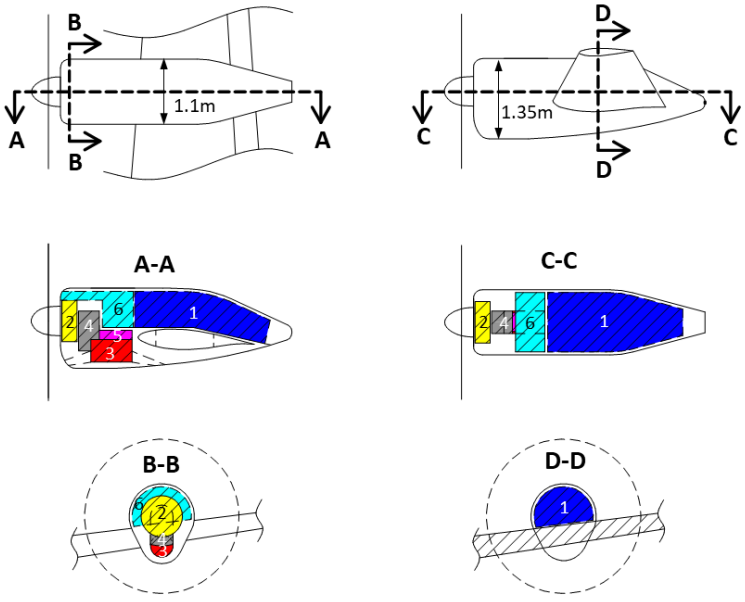

Nr	Component	Properties
1	Space for battery	Volume ≈ 1.0m^3
2	E-Motor	0.7m x 0.25m (D x L)
3	Gas Turbine	0.4m x 0.7m (D x L)
4	Gearbox (incl. clutch)	0.5m x 0.4m x 0.35m (L X W x H)
5	Gas turbine systems	0.5m x 0.3m x 0.15m (L X W X H)
6	Space for cooling system and power management system	Volume ≈ 0.25m^3

Figure 8: Space allocation of the propulsion system within the nacelle.

aircraft can operate on routes of up to 190 km. With reduced payload, fuel can be used for the mission as well. With a standard payload factor of 70% the aircraft can operate up to approximately 1000km in hybrid mode. More details regarding this will be provided in Section 5.3.2. Figure 9 also contains the payload range ISO-lines for different shaft power split between electric power and range extender power. E.g., the "50% Electric Power" boundary shows the mission distances possible when, on average, half of the propulsion power comes from the battery.

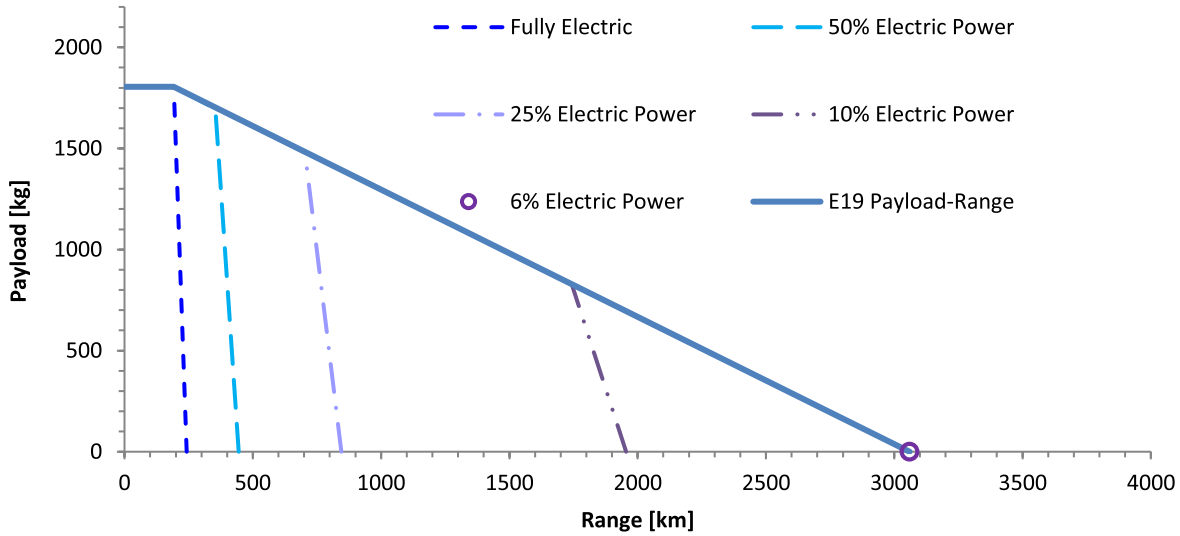

Figure 9: Payload-range diagram of the E19.

The aerodynamic performance of the E19 is illustrated in Figure 10. At electric cruise the aircraft operates at an L/D ratio of 19.3, whereas the best L/D ratio is 19.8. Additionally, the figure provides a more detailed drag breakdown for each of the aircraft components.

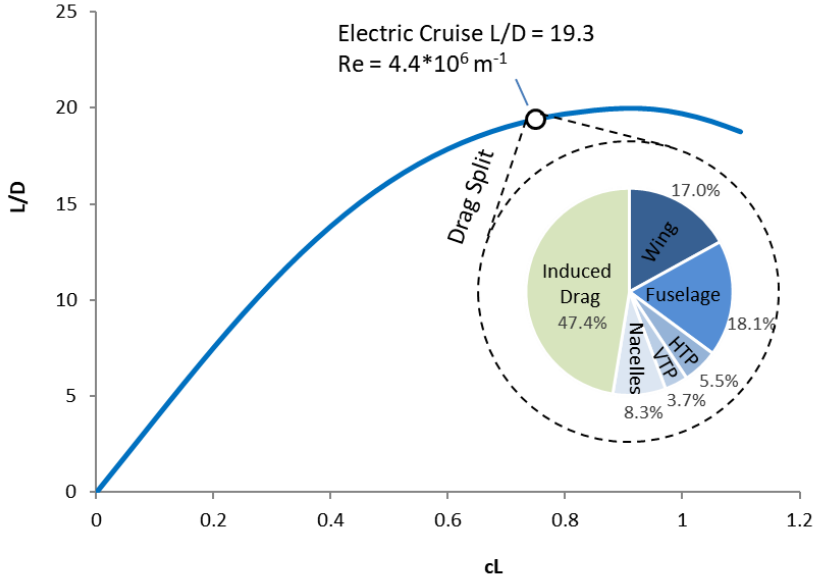

Figure 10: Aerodynamic polar of the E19 in the electric cruise condition.

5.3. Mission analysis

This section will present the mission analysis results for the E19. As the aircraft is capable of both full electric flight and hybrid flight, the results are divided subsequently.

5.3.1. All-electric missions

The E19 can fly missions up to 190km using electric energy only. For these missions, sufficient kerosene is carried on-board to be able to fulfil the required IFR reserves, but it is only used in case the aircraft cannot land safely within the fully electric range. Since the achievable range for the all-electric missions is close to 200km, the impact of flight speed on the mission time is relatively low. Therefore, the mission optimisation is set to heavily prioritize on range, resulting in lower cruise speeds of around 300km/h and lift coefficient values close to the best range performance. The shorter missions are carried out at an altitude of 3048m in order to avoid pressurisation of the cabin, which requires off-takes that reduce the performance of the aircraft. The off-take system of the E19 is assumed the same as for the Jetstream 31, thus requiring bleed air from the gas turbines. Therefore, with the current setup, altitudes higher than 3048m can only be serviced in hybrid operation mode. This design approach was selected to keep the design model simple. Alternative solutions should be implemented and analysed if all-electric operation above 3048m is considered relevant. The descent is assumed to be carried out unpowered with the propellers stopped in a feathered position. Figure 11 illustrates the power and altitude profile over time for an electric mission of the E19.

5.3.2. Hybrid-energy missions

Longer missions can be carried out by running the range extenders in parallel with the batteries. An optimized power management strategy needs to consider the efficiency of the different power providers during the mission; e.g. the gas turbines should not be running at low power load, as their efficiency is heavily penalized. A first solution may be to run the range extenders at or close to design power until the fuel dedicated for the main mission runs out, then proceeding only with battery power at an altitude of 3048m. Alternatively full optimisation studies can be made to find the optimal solution. As that is outside the scope of this conceptual study, the calculation model used is simple and considers a constant power split between the range extenders and the battery during cruise, regardless of the power loading of the components.

With the range extenders running, the aircraft can be pressurized using bleed air. Thus, the aircraft can climb higher in order to improve the speed performance, which is important for the longer missions. An example of such a mission profile is given in Figure 12. Since the range extenders are sized for loiter speeds at 3048m, they are not sufficient for achieving

high flight speeds without the support from the electric motors. Therefore, the aircraft can show its best performance in terms of speed at ranges between 200km and 400km (see Figure 11), where the battery energy is sufficient to provide a good portion of the total power, whereas the fully electric missions (under 200km for standard payload) prioritize performance at the cost of speed. For longer ranges, the battery power must be kept low in order for the battery to not be prematurely depleted, which results in lower aircraft velocities. This variation of the design speed with the range is synergetic with the needs of the 19-seater market. As shown in Figure 2, well over 50% of the missions are flown at distances below 200km, where any benefits from higher speed are strongly dampened by the Landing-Take-Off (LTO) cycle time of the aircraft. Furthermore, another 30% of the total missions are carried out at ranges from 200km to around 400km, where the E19 shows its peak performance in terms of speed.

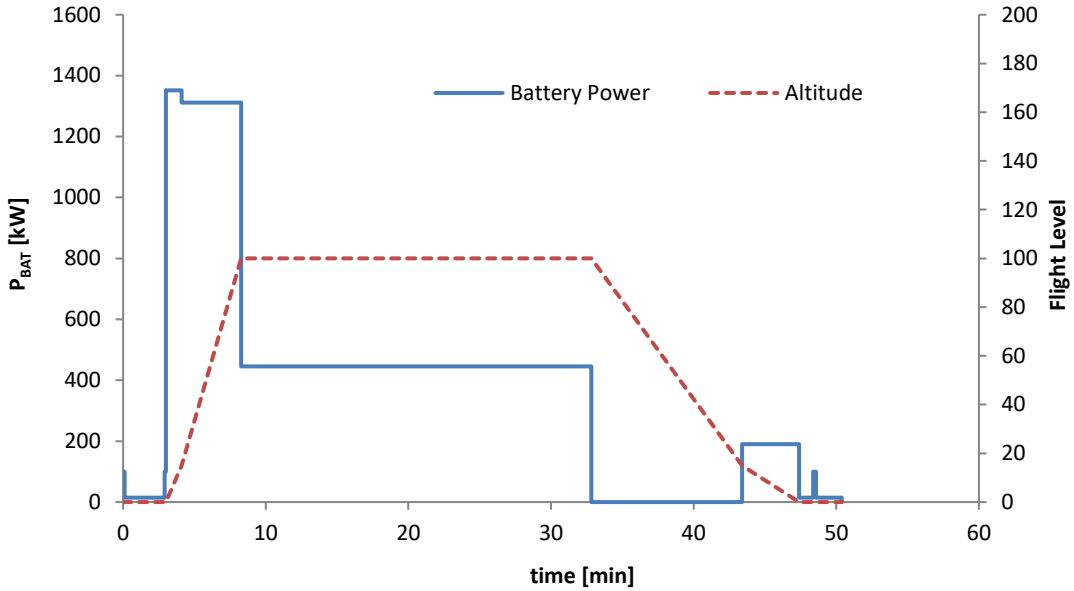

Figure 11: E19 all-electric mission profile example.

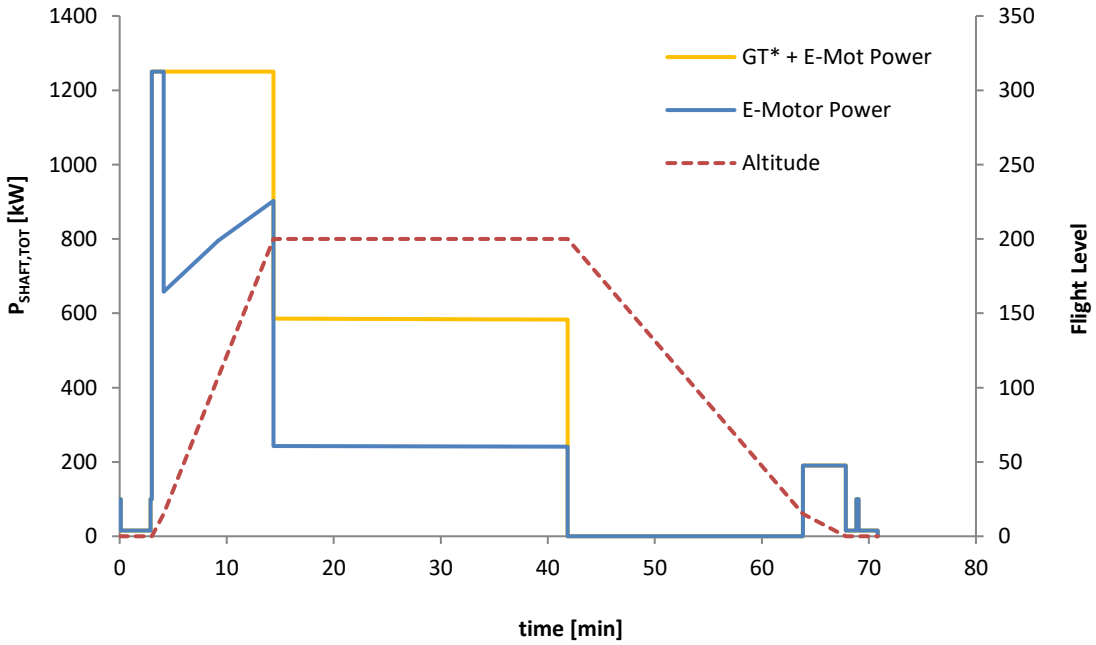

Figure 12: E19 hybrid mission profile for a 340km mission. *GT: Gas turbine*

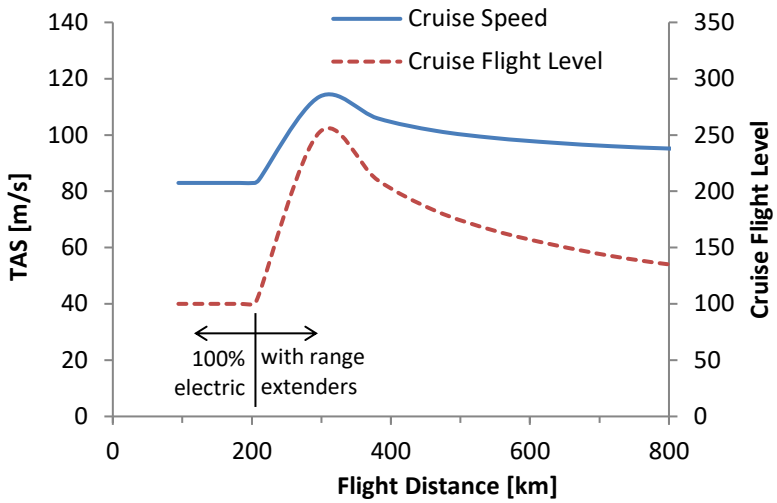

Figure 13: True air speed and flight level dependence on the flight distance set for the operation of the E19.

5.4. Operational aspects

The payload range diagram of the E19 is compared to that of the reference aircraft in Figure 14. In this figure the typical utilization marking is inferred from the diagram shown in Figure 2 with the assumption that the average payload is around 70% of the maximum seating capacity. In addition to the so far presented reference aircraft, the Viking Air DHC-6 Series 400 “Twin Otter” is also incorporated in the overview [53, 54, 55]. The Twin Otter is another representative for STOL utility aircraft and represents an important part of the 19-seater market. The penalized aircraft performance due to the STOL characteristics become clear through the steeper gradient at the payload-range boundary line in which payload is reduced. The E19 is slightly underperforming with its payload-range capabilities compared to the reference aircraft. Nevertheless, the E19 is able to service the typical utilization range of the market on top of being capable of full electric flight. The E19’s gradient of the range increase with payload reduction is comparable to the previously introduced reference aircraft. This gradient is an indicator of the overall fuel efficiency of the aircraft. Hence, despite the substantial mass penalty due to the fully electric flight capability, the E19 is comparable to the reference aircraft in terms of energy. The aerodynamic performance of the E19 is significantly better than that of the reference aircraft due to the relatively high values for the cruise lift coefficients (c.f. also Figure 10) and large wing span. Furthermore, the large wing of the E-19 enables a high storage volume for fuel and can utilize the battery energy as well, leading to a very high ferry range. Table 9 provides a comparison between the aircraft for a number of performance parameters.

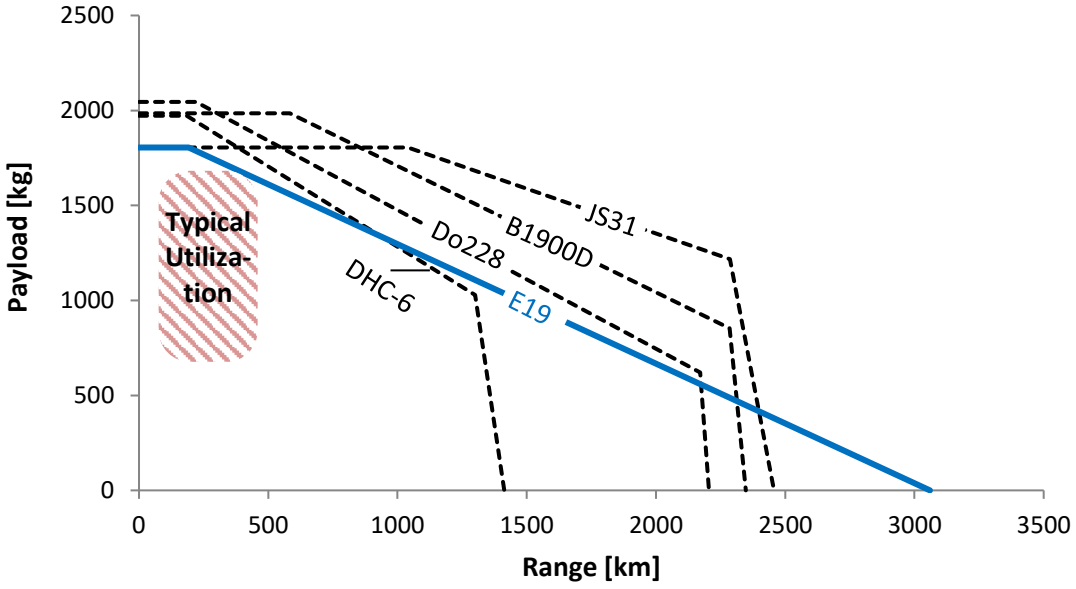

Figure 14: Payload-range diagram comparison of the E19 with different commuter aircraft.

Table 9: Overall performance parameters comparison between the E19 and the reference aircraft.

Parameter	Units	Do228	BAe JS31	B1900D	E19
MTOM	kg	6400	6950	7766	8618
Wing area	m2	32	25.2	28.8	33
Wing span	m	17	15.9	17.75	20
cL_{cruise}	-	0.3	0.55	0.45	0.75* / 0.63**
L/D_{cruise}	-	10.0	14.6	12.1	19.3* / 17.7**
$psfc_{GT,cruise}$	kg/kWh	0.34	0.32	0.33	0.35***

*In fully electric mode **In hybrid mode ***Range extender fuel consumption.

The high lift coefficient in cruise of the E19 is an indicator of the low speed of the aircraft. The reference aircraft are around 30% to 70% faster than the chosen all-electric cruise speed of the aircraft. However, this is not a capability issue of the E19, as it operates at only about one third of the available electric power in cruise, as shown in Figure 11. At higher power setting the cruise velocity can significantly increase, but the achievable range would decrease as a trade-off. As discussed in Section 5.3.1, the speed is optimized for the electric range since flight time is not a dominant operational performance factor for missions less than 200km. Rather, the LTO cycle time and passenger total travel time play a significant role there. Figure 15 provides a comparison in terms of mission time required with regard to airport-to-airport distance for the E19 and the reference aircraft. Assuming an LTO time of 20 minutes, the total mission time for a fully electric 200km mission is around 60 min for E19, which is approximately 10 minutes higher than for the Do228. For the longer missions, where cruise speed plays a more prominent role, the E19 assumes a hybrid operation with an increased velocity as shown in Figure 13. Therefore, the time penalty remains within 10 to 15 minutes for missions up to 400km, at which around 90% of the typical 19-seater utilization is reached. The slower, but still successful, STOL utility class representative Twin Otter is a further indicator that velocity is not a single dominant trait in this market.

The flight time, however, can have a significant effect on the operating costs of the aircraft. Another important aspect of the operations would be turnaround time, where battery recharging could become a bottleneck and negatively impact the time-related costs of the operation. With hybrid designs, there is always the option of using more kerosene than battery for a mission in order to reduce charging time and, thus, improve the operational flexibility. However, this would come at the cost of reducing the potential energy savings presented in Subsection 5.5.

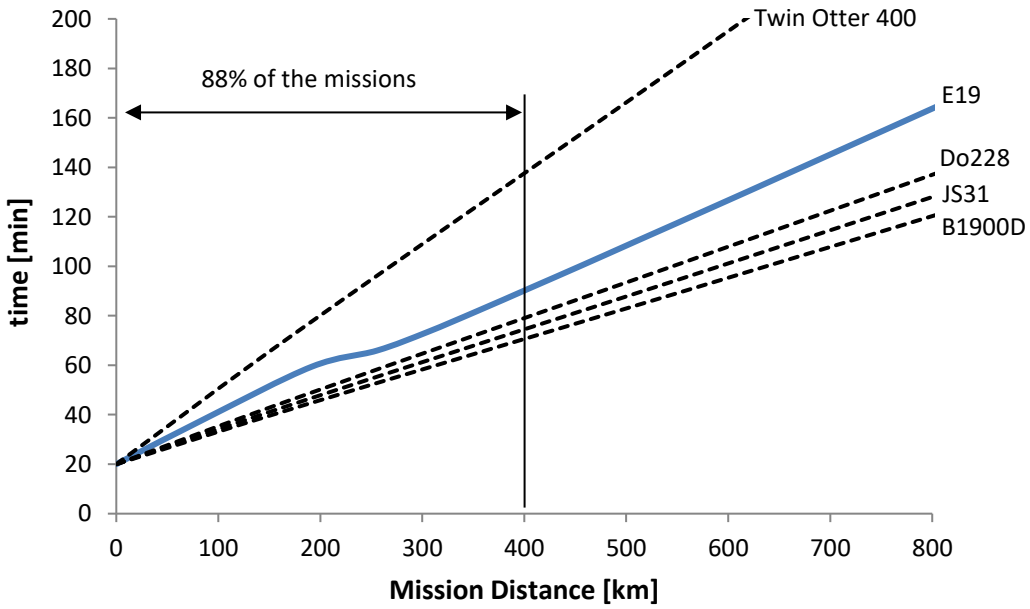

Figure 15: Mission time comparison between the E19 and various commuter aircraft for the typical utilization speed and an LTO cycle of 20 minutes.

Another operational aspect that needs more detailed modelling in future studies is the low-speed performance of the aircraft. Most 19-seater aircraft share a STOL capability, which allows the utilization of small commuter airports. Long take-off distance could limit the available airport options for the aircraft operator, which can be a significant drawback considering the comparatively long TOFL of E19 if a fully-electric take-off is assumed. However, the take-off performance of the aircraft can be potentially improved by combining both the electric motor power and the range extender power. An estimate of this effect, using the methodology described in Section 4.4.1, is provided in Table 10.

A proper assessment of the operational aspects would require a cost model, an airline operation model and detailed battery modelling including operational aspects and life cycle analysis. These were not within the scope of this study. Hence, the fleet-level energy efficiency results that will be presented in Subsection 5.5 are to be viewed as a more ideal assessment of the technology potential, since practical aspects from the aircraft operations will tend to eat away from the energy performance. The results sensitivities discussion that will be presented in Subsection 5.6 can be used for a preliminary risk assessment in this regard.

Table 10: Speed and take-off capability comparison of the E19 with the reference aircraft and the Twin Otter.

Aircraft	Cruise Speed [kts]	TOFL (MTOM, ISA) [m]
E19 (electric mode)	160	1440
E19 (hybrid mode)	175 - 210	850
Do228NG	234	800
Bae JS31	263	1440
B1900D	277	1140
Twin Otter 400	112	454

5.5. Fuel efficiency and emission reduction potential

Fuel efficiency, especially at the short ranges operated on by 19-seater aircraft, is the dominant design trait of the E19. A comparison between the hybrid aircraft and the Do228, which can be seen in Figure 16, shows a considerable kerosene burn reduction potential in the most relevant operational range of up to 400km. Even at the higher ranges, the fuel efficiency benefit is significant. To ensure a fair comparison in Figure 16, the E19 is compared to both the "maximum cruise speed" and the "long-range cruise" operation mode of the Do228.

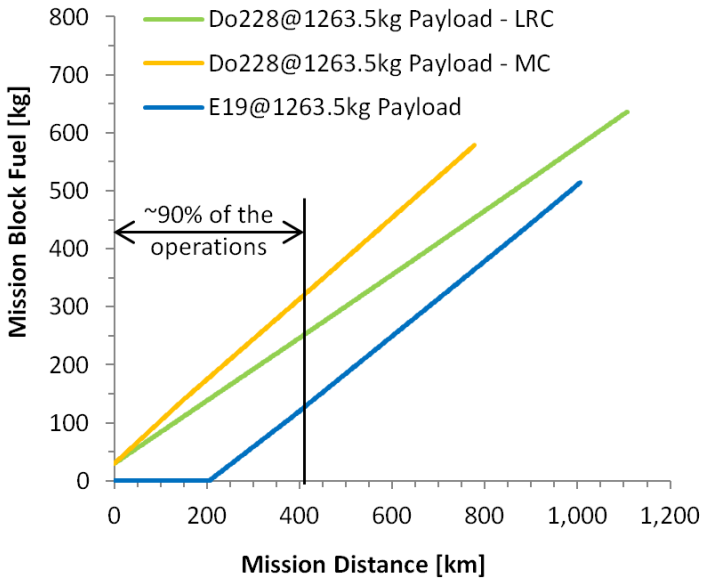

Figure 16: Block fuel comparison between the E19 and the Do228.
MC: maximum cruise speed; LRC: long-range cruise speed

Reference [12] provides a fuel performance comparison between the E19 and the Do228 on global fleet level. This is achieved by assuming that the global 19-seater aircraft fleet is operated by only one aircraft model, i.e. either the Do228 or the E19, and consequently comparing the overall fuel burned by each corresponding fleet for all operated routes over the course of an entire year. The comparison shown in [12] yields a potential of 70% fuel reduction when the fleet is

operated only by the E19 compared to a fleet comprised only of Do228 aircraft operated at fuel-efficient speeds. A qualitative overview of these results is shown in Figure 17, which combines the 19-passenger fleet flight frequency distribution over the flight distance provided in [12] and shown in Figure 2 with the block fuel performance shown in Figure 16.

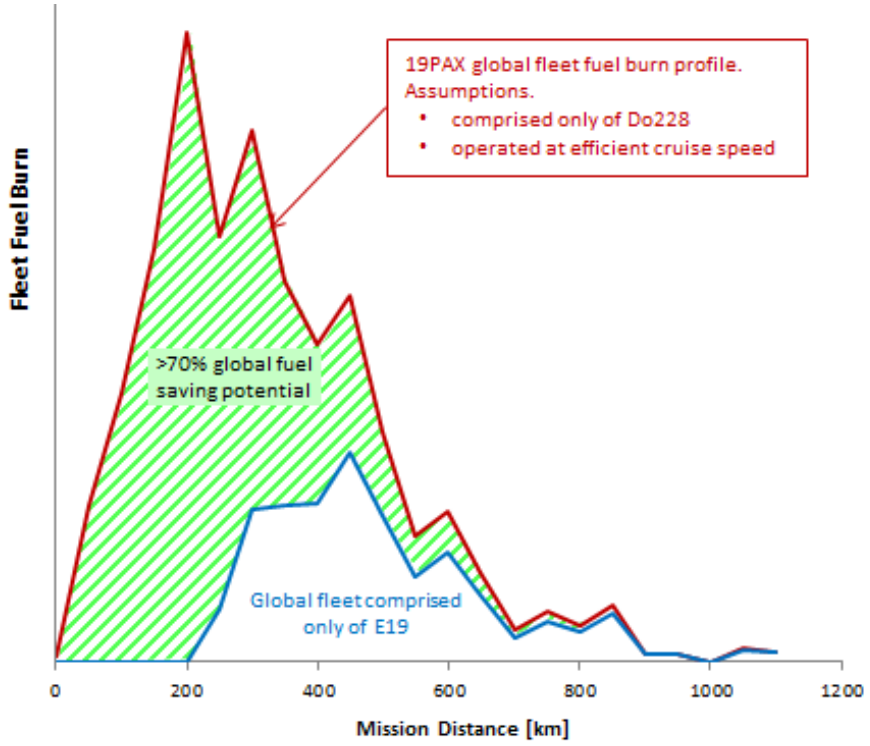

Figure 17: Fleet-level fuel saving potential of the E19 compared to a conventional turboprop.

Fuel consumption reduction would translate almost directly into environmental impact reduction if renewable energy sources assumed for charging the battery in operation as well as for the battery life cycle energy needs. Electric power production, however, has a significant CO_2 footprint. Data from the German Federal Ministry for Economic Affairs and Energy reveals that 1kWh electric energy provided by the German power grid caused approximately 474gCO_2 emissions in 2019 [56]. In comparison, burning 1kWh worth of kerosene amounts to approximately 264gCO_2 emissions. Furthermore, the battery production causes additional emissions. Reference [57] specifies that production amounts to approximately 17kgCO_2 equivalent emissions per kg of produced battery. Using the effective specific energy and the end-of-life cycles of the battery pack model used for the E19 (see Section 4.3), the emissions due to production results in approximately 100gCO_2 per kWh battery output. Recycling is typically accounted for in the production figures, which tends to reduce the overall footprint [58]. Therefore, 100gCO_2-eq/kWh is assumed for both production and recycling of the batteries, resulting in a total footprint of 574gCO_2-eq/kWh for the electric energy used by the battery. However, crude oil-based fuel production and logistics cause a similar footprint – e.g., around 56gCO_2 per kWh worth of diesel [59]. Assuming the same production and logistics footprint for kerosene and adding the value to the combustion emissions results in a total footprint of 320gCO_2-eq/kWh. Therefore, combining the fleet kerosene consumption profiles shown in Figure 16 and the electric energy consumed by the E19 with the derived footprint values results in a total of 50% CO_2 emissions reduction for an E19 fleet compared to a Do228 fleet, which is shown in Figure 18. Figure 19 provides an explanation of the shown significant CO_2 footprint improvement potential of electric flight, with the main reasons being:

- The total efficiency of the electric chain amounts to over 80%, whereas the gas turbine efficiency of the Do228 is around 25%. Therefore, the CO_2 footprint of the propulsion shaft power provided by the electric chain is around 685gCO_2-eq/kWh, whereas the footprint of the turboprop shaft power is much higher – approximately 1280gCO_2-eq/kWh.
- The energy consumption in the idle power phases (taxi, descent, etc.) is reduced by an order of magnitude with electric propulsion and their contribution is significant for the typically short distances flown by the commuter aircraft.

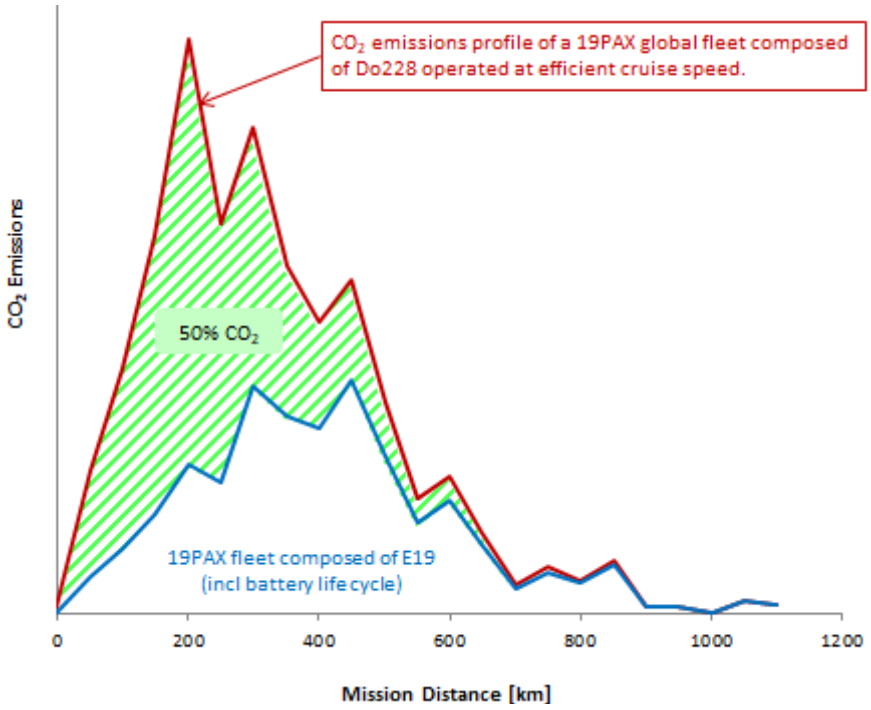

Figure 18: Fleet-level CO_2 emissions saving potential of the E19 compared to a conventional turboprop.

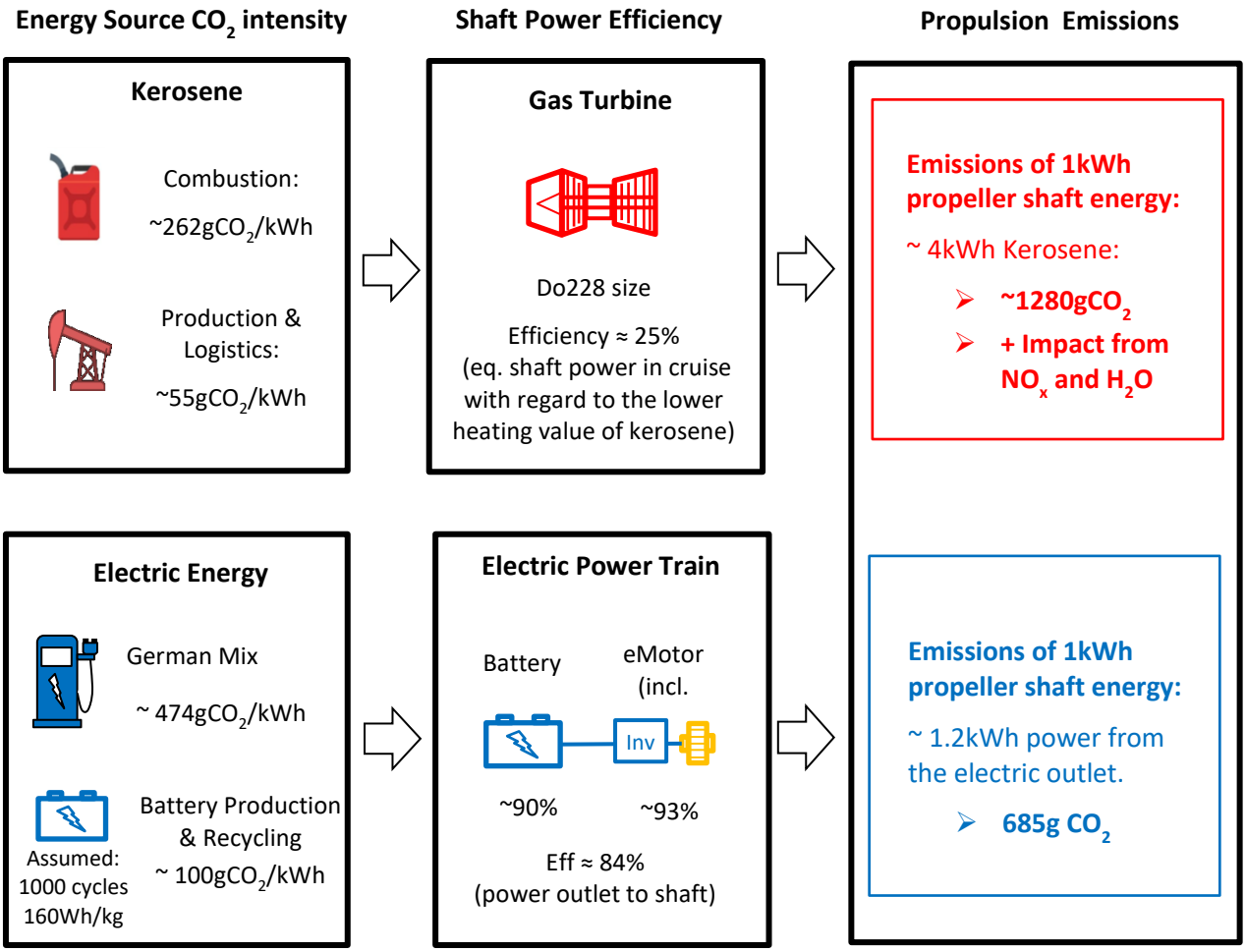

Figure 19: Comparison of the emissions of kerosene with the emissions of an electric flight.

5.6. Results sensitivities

The results presented for the conceptual design are bound to the modelling assumptions described in Section 4. The described study has been performed on a conceptual level, which carries the risk of overestimating or underestimating important aspects of the design. In order to quantify the dependency of the results on such uncertainties, a results sensitivity study was performed.

As shown in Figure 20, a change in the aerodynamic efficiency of the aircraft will have some effect on the results. However, even if the aerodynamic efficiency is over- or underestimated by around 10%, the overall outcome of the study does not change significantly. It is similar with the specific energy assumption of the battery pack. Even if a reduction of the specific energy of 25% significantly reduces the all-electric range, the overall fuel needed for normal fleet operation is still more than halved.

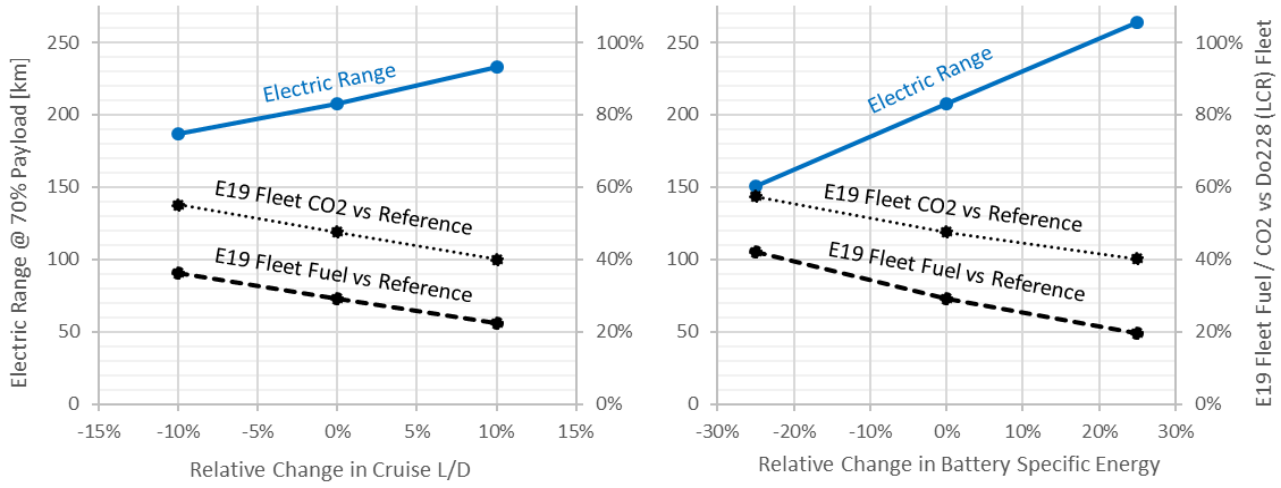

Figure 20: Results sensitivities on aerodynamics and battery specific energy.

As mentioned in Subsection 5.1,the low-speed performance assessment was not a focus of the design, which imposes significant uncertainties with regard to the wing sizing. If the take-off performance of current design is underestimated, a possible mitigation measure would be to increase the wing size, which would improve both take-off and landing performance. A sensitivity trade on the wing size, assuming the same propulsion system, is shown in Figure 21. Increasing the wing size by 10% also increases wing mass and the mass of the empennage, which is dependent on the wing size (see Section 4.2). This leads to an increased MZEM of the aircraft, resulting in 2.5% less battery mass that can be installed due to the fixed MTOM of 8618kg. However, the effect on the electric range is dampened by the improved L/D of the aircraft, which results from the bigger span and the decreased portion of total wetted area to wing reference area. Hence, the overall performance of the aircraft is not significantly affected by wing size. The highest impact of wing size is on the cruise speed of the aircraft, which needs to be decreased by around 5% in order to maintain the cruise performance optimisation constraint described in Subsection 5.3. This can have a considerable effect on operating costs of the aircraft. However, the assessment of the operating costs is not in the scope of the study.

A variation of the Zero-Energy Empty Mass (ZEEM), which is the OEM without the battery, can have a significant impact on the overall design of the aircraft. Adding a mass penalty of 10% of the ZEEM, which is around 400kg, results in roughly 20% less battery that can be installed without exceeding the MTOM limit of 8618kg. The penalty on the battery mass is somewhat dampened by a reduced nacelle size. However, since the specific power of the battery is fixed, the battery power constraint shown in Figure 6 is shifted towards 20% lower take-off power, ultimately resulting in around 20% increase in wing reference area for meeting the TOFL constraint. Therefore, an increase in ZEEM impacts not only the overall energy efficiency of the concept due to the reduced electric range but also leads to a significant cruise speed penalty. This sensitivity trade shows the importance of minimizing the airframe mass for electric aircraft. If major components of the E19 design were designed with lightweight materials instead of the old airframe technology of commuter aircraft from the 80's, the overall performance of the concept can be boosted significantly. However, such a redesign was not in the scope of the current study.

The importance of the ZEEM with regard to the overall performance is also an indicator that the early design decision to include a pressurized cabin to allow for faster operation in hybrid mode takes a significant toll on the overall performance due to the ZEEM penalty. An unpressurized cabin design is probably the better option for the state-of-the art battery technology assumed for this study. Nevertheless, a pressurized cabin is probably the better option in the longer term, since

outdated batteries can be replaced with better ones in the future. As can be seen in Figure 20, future batteries with improved specific energy would allow for a longer electric range, where the importance of a faster high-altitude cruise on the overall mission time and, thus, on the operating costs increases.

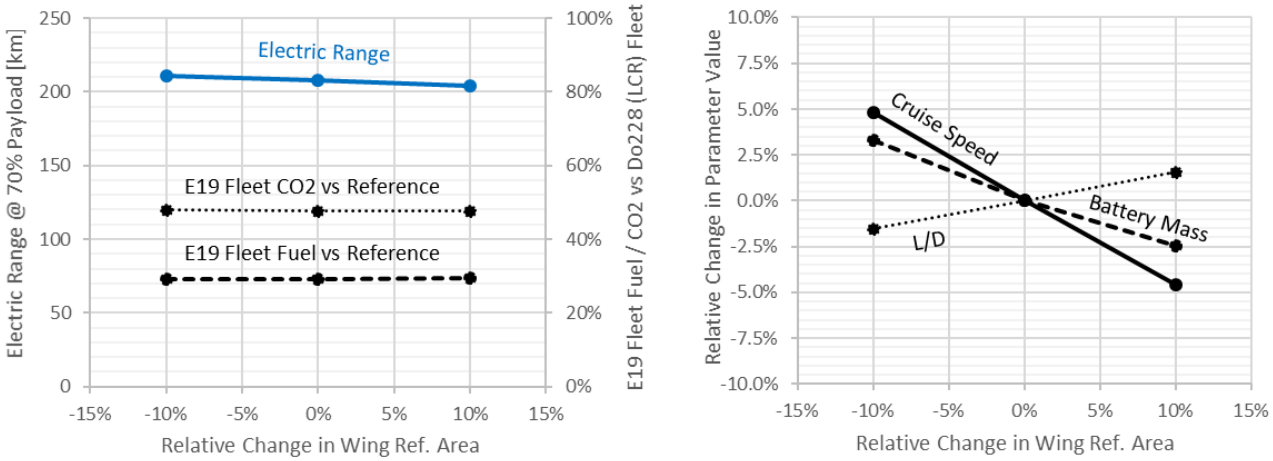

Figure 21: Results sensitivities on wing reference area with constant take-off power.

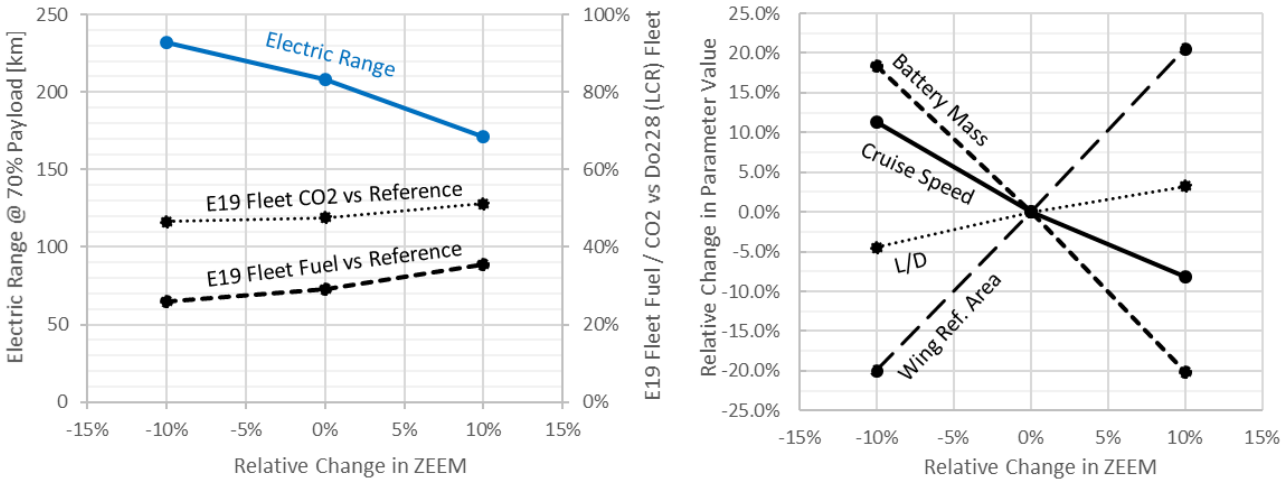

Figure 22: Results sensitivities on the zero-energy empty mass (ZEEM).

6. CONCLUSIONS

This paper provides the conceptual aircraft design results from a collaborative project between the DLR and Bauhaus Luftfahrt, in which the potential of a hybrid-electric commuter aircraft was investigated. The resulting aircraft is a 19-seater commuter aircraft, named E19, capable of fully electric flight. The design has been specifically tailored for the commuter aircraft operation needs. A market analysis, which was part of the same project, showed a large amount of commuter aircraft missions is flown on a relatively short range. This opens up the possibility for full electric flight on most of the shorter missions, whereas the combustion-based range extenders allow more operational flexibility and provide the required reserve mission capabilities.

Using openAD as the aircraft design framework, the models used for the design and assessment were calibrated on existing commuter aircraft that share a similar configuration and characteristics as the E19 to ensure reliability of the results. However, also due to this reason, the aircraft assessment remains on the conservative side, as turboprop aircraft technology of the 80s is implicitly assumed in the results. The full potential of the technology could be better understood if the E19 is designed for state-of-the-art airframe technology and compared to a respective design of a conventional turboprop. Furthermore, the overall aircraft modelling should also include a more detailed analysis of the propulsion chain

behaviour during operation, as well as space allocation modelling for the integration into the aircraft, both of which are simplified for this study.

The resulting aircraft design has a full electric range of 190km, allowing it to serve around 50% of the commuter operations in-flight emissions free. When using the range extenders, the aircraft is capable to provide similar ranges as the refence aircraft, although at a lower payload mass. The flight time of the E19 is up to around 20 minutes longer compared to reference aircraft for missions up to 400km. Nevertheless, the assessment of the aircraft concludes that by using a hybrid chain with a range-extender approach, state-of-the-art technology has sufficiently advanced to enable an aircraft with fully electric flight capability, which can offer a competitive operational performance and a significant fuel burn reduction potential. In collaboration with a market study on thin-haul commuter aircraft [12], it was shown that potentially more than 70% fuel burn and more than 50% CO_2 emissions reduction can be achieved on fleet level if all 19-seater class commuter flights were operated by the E19. However, besides the technical performance also the financial performance plays an important role. Hence, the analysis should be expanded to include an operator's cost model to assess the competitiveness potential of the aircraft on this market further and to draw final conclusions on the feasibility.

NOMENCLATURE

Abbreviations

BAe	British Aerospace	LTO	Landing-Take-Off Cycle
CAS	Calibrated AirSpeed	MAC	Mean Aerodynamic Chord
CoCoRe	Cooperation for Commuter Research (project)	MLM	Maximum Landing Mass
CoG	Centre of Gravity	MTOM	Maximum Take-Off Mass
CS	Certification Specifications	MZEM	Maximum Zero Energy Mass
DLR	Deutsches Zentrum für Luft- und Raumfahrt / German Aerospace Center	OEM	Operating Empty Mass
Do	Dornier	SoC	State of Charge
ECS	Environmental Control System	STOL	Short Take-Off and Landing
GT	Gas Turbine	TAS	True AirSpeed
HTP	Horizontal TailPlane	TLARs	Top Level Aircraft Requirements
IFR	Instrument Flight Rules	TOFL	Take-Off Field Length
JS	JetStream	TOP	Take-Off Performance
IFR	Instrument Flight Rules	VTP	Vertical TailPlane
LoD	Lift over Drag (ratio)	ZEEM	Zero-Energy Empty Mass
LTH	LuftfahrtTechnische Handbuch	ZFM	Zero Fuel Mass

REFERENCES

[1] European Commision, "Flightpath 2050: Europe's Vision for Aviation," Publications Office of the European Union, Luxembourg, 2011.

[2] ICAO, "Doc 10126, CAEP/11," Montréal, 2019.

[3] A. W. Schäfer, A. D. Evans, T. G. Reynolds and D. Lynette, "Costs of Mitigating CO2 Emissions from Passenger Aircraft," *Nature Climate Change,* vol. 6, no. 4, pp. 412-417, 2016.

[4] Airbus, "Global Market Forecast 2019: Cities, Airports & Aircraft 2019-2038," Airbus S.A.S., Blagnac Cedex, 2019.

[5] Boeing, "Commercial Market Outlook 2020-2039," Boeing, 2020.

[6] C. Pornet and A. T. Isikveren, "Conceptual design of hybrid-electric transport aircraft," *Progress in Aerospace Sciences,* vol. 79, pp. 114-135, 2015.

[7] National Academy of Engineering Committee on Propulsion and Energy Systems, "Commercial Aircraft Propulsion and Energy Systems Research: Reducing Global Carbon Emissions," National Academies Press, 2016.

[8] M. A. Stoll and G. V. Mikic, "Design Studies of Thin-Haul Commuter Aircraft with Distributed Electric Propulsion," in *16th AIAA Aviation Technology, Integration, and Operations Conference*, Washington, D.C., 2016, https://doi.org/10.2514/6.2016-3765.

[9] M. D. Moore, "Misconceptions of Electric Aircraft and their Emerging Aviation Markets," in *52nd Aerospace Sciences Meeting*, National Harbor, Maryland, USA, 2014.

[10] A. T. Isikveren, A. Seitz, P. C. Vratny, C. Pornet, K. O. Ploetner, M. Hornung and B. L. V, "Conceptual Studies of Universally-Electric Systems Architectures Suitable for Transport Aircraft," in *61. Deutscher Luft- und Raumfahrtkongress*, Berlin, Germany, 2012.

[11] A. R. Gnadt, R. L. Speth, J. S. Sabnis and S. R. Barrett, "Technical and environmental assessment of all-electric 180-passenger commercial aircraft," *Progress in Aerospace Sciences,* vol. 105, no. 16, pp. 1-30, 2019.

[12] A. Paul, W. Grimme, G. Atanasov, J. van Wensveen and F. Peter, "Evaluation of the Market Potential and Technical Requirements for Thin-Haul Air Transport," German Aerospace Congress 2019, Darmstadt, 2019, https://doi.org/10.25967/490206.

[13] W. Grimme, A. Paul, S. Maertens and J. van Wensveen, "The prospects of hybrid-electric regional air transport - an assessment of travel time benefits of domestic short-haul flights in Germany with 19-

seater aircraft," *Transportation Research Procedia,* vol. 51, pp. 199-207, 2020, https://doi.org/10.1016/j.trpro.2020.11.022.

[14] B. J. Brelje and J. R. Martins, "Electric, Hybrid, and Turboelectric Fixed-Wing Aircraft: A Review of Concepts, Models, and Design Approaches," *Progress in Aerospace Sciences,* vol. 104, pp. 1-19, 2019.

[15] Y. Fefermann, C. Maury, C. Level, K. Zarati, J.-P. Salanne, C. Pornet, B. Thoraval and A. T. Isikveren, "Hybrid-Electric motive power systems for commuter transport applications," in *Proceedings of the 30th Congress of the International Council of the Aeronautical Sciences*, Daejeon, Korea, 2016.

[16] P. G. Juretzko, M. Immer and J. Wildi, "Performance Analysis of a Hybrid-Electric Retrofit of a Ruag Dornier Do-228NG," in *66. Deutscher Luft- und Raumfahrtkongress*, Munich, Germany, 2017.

[17] G. Tay, P. Keller and M. Hornung, "Development of a software tool for comprehensive flight performance and mission analysis of hybrid-electric aircraft," *Transportation Research Procedia,* vol. 29, no. 4, p. 401–409, 2018.

[18] M. Kreimeier and E. Stumpf, "Benefit evaluation of hybrid electric propulsion concepts for CS-23 aircraft," *CEAS Aeronautical Journal,* vol. 8, no. 4, p. 691–704, 2017.

[19] M. Kruger, S. Byahut, A. Uranga, J. Gonzalez, D. K. Hall and A. Dowdle, "Electrified Aircraft Trade-Space Exploration," in *2018 Aviation Technology, Integration, and Operations Conference*, Atlanta, Georgia, 2018.

[20] D. F. Finger, R. d. Vries, R. Vos, C. Braun and C. Bil, “A Comparison of Hybrid-Electric Aircraft Sizing Methods,” in *American Institute of Aeronautics and Astronautics (Hg.) 2020 – AIAA Scitech 2020 Forum*, Orlando, FL, USA, 2020.

[21] R. Jansen, C. Bowman and A. Jankovsky, "Sizing Power Components of an Electrically Driven Tail Cone Thruster and a Range Extender," in *American Institute of Aeronautics and Astronautics (Hg.) 2016 – 16th AIAA Aviation Technology*, Washington, D.C., 2016.

[22] F. Orefice, F. Nicolosi, P. Della Vecchia and D. Ciliberti, "Conceptual Design of Commuter Aircraft including Distributed Electric Propulsion," in *AIAA Aviation Forum*, Virtual event, 2020.

[23] "Ruag to relaunch Do 228 production," AIN online, 28 12 2007. [Online]. Available: https://www.ainonline.com/aviation-news/aviation-international-news/2007-12-28/ruag-relaunch-do-228-production. [Accessed 25 09 2019].

[24] "Beech 1900 Airliner," GlobalSecurity.org, 07 07 2011. [Online]. Available: https://www.globalsecurity.org/military/systems/aircraft/be1900.htm. [Accessed 25 09 2019].

[25] RUAG, "Dornier 228 Advanced Commuter (AC) Facts & Figures," 2015.

[26] Janes All the World's Aircraft 2011-2012, ISBN-13 978 0 7106 29555, 2011.

[27] EASA Type-certificate data sheet, Dornier 228 Series, Issue 5, European Aviation Safety Agency, 2017.

[28] Janes All the World's Aircraft 1980-1981, ISBN 0 7106-0705-9, 1980.

[29] EASA Type-certificate data sheet, Jetstream 3100/3200 Series, Issue 2, European Aviation Safety Agency, 2009.

[30] Flygunderhållsystem Beech 1900D, Rapportkod: MDH.IDT.FLYG.0195.2008.GN300.15HP.M, 2008.

[31] Type certificate data sheet No. A24CE, Revision 67, Department of Transportation, Federal Aviation Administration, 1998.

[32] Janes All the World's Aircraft 2004-2005, ISBN-13 978-0710626141, 2004.

[33] A. K. Cooke, A Simulation Model of the NFLC Jetstream 31, Cranfield: Cranfield University, 2006.

[34] S. Wöhler, G. Atanasov, D. Silberhorn and B. Fröhler, "PRELIMINARY AIRCAFT DESIGN WITHIN A MULTI-DISCIPLINARY AND MULTI-FIDELITY DESIGN ENVIRONMENT," in *Aerospace Europe Conference*, Bordeaux, 2020.

[35] E. Torenbeek, Synthesis of Subsonic Airplane Design, Kluwer Academic Publishers, 1982.

[36] J. Roskam, Airplane Design, Part V: Component Weight Estimation, Ottawa, Kansas: Roskam Aviation and Engineering Corporation, 1985.

[37] D. P. Raymer, Aircraft Design: A Conceptual Approach, Second Edition, Washington, DC: AIAA Education Series, 1989.

[38] v.Braur and Wissel, "Tragwerk Tansporter Statistische Massenabschätzung," Luftfahrttechnisches Handbuch (LTH), 1998.

[39] D. P. Wells, B. L. Horvath and L. A. McCullers, "The Flight Optimization System Weights Estimation Method," National Aeronautics and Space Administration (NASA), 2017.

[40] J. Roskam, Aircraft Design, Part VI: Preliminary Calculation of Aerodynamic, Thrust, and Power Characteristics, Ottawa, Kansas: Roskam Aviation and Engineering Corporation, 1987.

[41] Janes All the World's Aircraft 1988-1989, ISBN 0 7106-0867-5, 1988.

[42] "Siemens eAircraft. Disrupting the Way You Fly.," 27 04 2018. [Online]. Available: https://www.ie-net.be/sites/default/files/Siemens%20eAircraft%20-%20Disrupting%20Aircraft%20Propulsion%20-%20OO%20JH%20THO%20-%2020180427.cleaned.pdf. [Accessed 26 09 2019].

[43] M. Emmerich, "Battery Assembly and Packaging for Aviation Applications," Fourth E2Flight Symposium, Stuttgart, 2019.

[44] TYVA, "Eraole Hybrid Electric Aircraft," TYVA, [Online]. Available: https://tyva-moduloo.com/project/eraole-hybrid-electric-aircraft/. [Accessed 24 02 2021].

[45] TYVA, "3D AX New High Capacity Battery," TYVA, [Online]. Available: https://tyva-moduloo.com/modular-lithium-battery-unit-systems-and-solutions/3d-ax-new-high-capacity-battery/. [Accessed 24 02 2021].

[46] U. Maier and M. Deutsch, "The Future Cost of Electricity-Based Synthetic Fuels," 16 May 2018. [Online]. Available: https://www.agora-verkehrswende.de/fileadmin/Projekte/2017/Die_Kosten_synthetischer_Brenn-_und_Kraftstoffe_bis_2050/Agora_SynCost_Webinar_slides_Deutsch_and_Maier_20180516.pdf. [Accessed 26 March 26].

[47] Siemens, "Elektrisches Fliegen," 18 06 2019. [Online]. Available: https://press.siemens.com/global/de/feature/elektrisches-fliegen. [Accessed 26 09 2019].

[48] Fraunhofer IISB, "Bidirectional full SiC 200 kW, DC-DC Converter for Electric, Hybrid and Fuel Cell Vehicles," 2015. [Online]. Available: https://www.mikroelektronik.fraunhofer.de/content/dam/mikroelektronik/Datenbltter/IIS_60kW_DB.pdf. [Accessed June 2019].

[49] H. Kellermann, M. Lüdemann, M. Pohl and M. Hornung, "Design and Optimization of Ram Air–Based Thermal Management Systems for Hybrid-Electric Aircraft," *Aerospace,* vol. 8, no. 1:3, p. https://doi.org/10.3390/aerospace8010003, 2021.

[50] K. Petermaier, "Electric propulsion components with high power densities for aviation," SIEMENS, 2015. [Online]. Available: https://nari.arc.nasa.gov/sites/default/files/attachments/Korbinian-TVFW-Aug2015.pdf. [Accessed 24 02 2021].

[51] Honeywell Aerospace, "TPE331-10 Turboprop Engine - Advanced engine performance and power generation capability," 2016. [Online]. Available: https://aerospace.honeywell.com/content/dam/aero/en-us/documents/learn/products/engines/brochures/N61-1491-000-000-TPE331-10TurbopropEngine-bro.pdf. [Accessed 24 02 2021].

[52] J. Roskam, AIRPLANE DESIGN, PART I: PRELIMINARY SIZING OF AIRPLANES, Ottawa, Kansas: Roskam Aviation and Engineering Corporation, 1985.

[53] Viking Air, *Twin Otter Series 400 technical specifications & standard equipment,* DOCUMENT REVISION: 01-18 ed., 2018.

[54] Aviation Week, "Purchase planning handbook," *Business & Commercial Aviation,* vol. 113, no. 5, 2017.

[55] European Aviation Safety Agency, *Type-Certificate Data Sheet DHC-6 Series 400,* 2017.

[56] Umweltbundesamt, "Climate Change 10/2019: Entwicklung der spezifischen Kohlendioxid-Emissionen des deutschen Strommix in den Jahren 1990 - 2018," October 2019. [Online]. Available: https://www.umweltbundesamt.de/sites/default/files/medien/1410/publikationen/2019-04-10_cc_10-2019_strommix_2019.pdf. [Accessed 12 March 2020].

[57] Fraunhofer ISE, "Treibhaushas-Emissionen für Batterie- und Brennstoffzellenfahrzeuge mit Reichweiten über 300km," 13 July 2019. [Online]. Available: https://www.ise.fraunhofer.de/content/dam/ise/de/documents/news/2019/ISE_Ergebnisse_Studie_Treibhausgasemissionen.pdf. [Accessed 24 March 2020].

[58] H. Melin, "Analysis of the climate impact of lithium-ion batteries and how to measure it," July 2019. [Online]. Available: https://www.transportenvironment.org/sites/te/files/publications/2019_11_Analysis_CO2_footprint_lithium-ion_batteries.pdf. [Accessed 24 03 2020].

[59] R. Edwards, D. Larive, D. Rickeard and W. Weindorf, "Well-To-Tank Report Version 4.a JEC Well-to-Wheels Analysis," 2014. [Online]. Available: https://publications.jrc.ec.europa.eu/repository/bitstream/JRC85326/wtt_report_v4a_april2014_pubsy.pdf. [Accessed 24 03 2020].

[60] PILOT'S OPERATING HANDBOOK, Do228-212, Edition 1, Revision 3, Fairchild Dornier, 2000.